NASA TECHNICAL MEMORANDUM

NASA TM X-2478

NASA TM X-2478

CASE FILE COPY

FLIGHT INVESTIGATION OF AN UNDERWING NACELLE INSTALLATION OF THREE VARIABLE-FLAP EJECTOR NOZZLES

by Verlon L. Head

Lewis Research Center
Cleveland, Ohio 44135

NATIONAL AERONAUTICS AND SPACE ADMINISTRATION • WASHINGTON, D. C. • JANUARY 1972

1. Report No.	2. Government Accession No.	3. Recipient's Catalog No.
NASA TM X-2478		

4. Title and Subtitle	5. Report Date
FLIGHT INVESTIGATION OF AN UNDERWING NACELLE INSTALLATION OF THREE VARIABLE-FLAP EJECTOR NOZZLES	January 1972
	6. Performing Organization Code
7. Author(s)	8. Performing Organization Report No.
Verlon L. Head	E-6564
	10. Work Unit No.
9. Performing Organization Name and Address	764-74
Lewis Research Center National Aeronautics and Space Administration Cleveland, Ohio 44135	11. Contract or Grant No.
	13. Type of Report and Period Covered
12. Sponsoring Agency Name and Address	Technical Memorandum
National Aeronautics and Space Administration Washington, D. C. 20546	14. Sponsoring Agency Code

15. Supplementary Notes

16. Abstract

A modified F-106B aircraft with underwing engine nacelles was flight tested to investigate airframe installation effects on three variable-flap ejector nozzles. Nozzle thrust coefficients, boattail drag coefficients, and boundary-layer characteristics were obtained for the three nozzles. All the nozzles were geometrically similar and had 15^{o} conical boattails with juncture radii of curvature equal to 0.5 maximum nozzle diameter. The effects of boattail location relative to the wing trailing edge and the ejector- to primary-nozzle-exit-diameter ratio were investigated. Shortening the length by 0.48 nozzle diameter lowered the transonic boattail drag rise Mach number from 0.97 to 0.95. Decreasing the nozzle exit diameter, which reduced the ejector- to primary-nozzle-exit-diameter ratio from 1.30 to 1.18, increased the gross thrust coefficient 4.8 percent.

17. Key Words (Suggested by Author(s))

Airframe installation effects; Propulsion system; Flight test; Underwing nacelles; Nozzle installation; Variable-flap ejector nozzle

18. Distribution Statement

Unclassified - unlimited

19. Security Classif. (of this report)	20. Security Classif. (of this page)	21. No. of Pages	22. Price*
Unclassified	Unclassified	47	$3.00

*For sale by the National Technical Information Service, Springfield, Virginia 22151

FLIGHT INVESTIGATION OF AN UNDERWING NACELLE INSTALLATION OF THREE VARIABLE-FLAP EJECTOR NOZZLES

by Verlon L. Head

Lewis Research Center

SUMMARY

A flight test program was conducted using a modified F-106B aircraft with underwing engine nacelles to investigate airframe installation effects on a variable-flap ejector nozzle. Nozzle gross thrust coefficients, boattail drag coefficients, and boundary-layer characteristics were obtained for three nozzles with 15^{o} conical boattails and boattail juncture radii of curvature equal to 0.5 nozzle diameter. Comparisons are made to a basic nozzle configuration with a projected boattail area equal to 54.8 percent of the nozzle maximum projected area. The two nozzles tested and compared with the basic nozzle were a shortened nozzle with the exit 0.48 nozzle diameter closer to the primary exit and a smaller exit area nozzle which increased the boattail area to 62.8 percent of the nozzle area. All other dimensions were the same as the basic nozzle. All three nozzles were tested at nonreheat and reheat power settings.

Shortening the ejector nozzle by 0.48 nozzle diameter lowered the drag rise Mach number from 0.97 to 0.95. Decreasing the nozzle exit diameter, which reduced the ejector- to primary-nozzle-exit-diameter ratio from 1.30 to 1.18, increased the gross thrust coefficient 4.8 percent at Mach 0.9. Relocation of two of the six rake positions indicated there is an even greater circumferential variation in nacelle boundary-layer characteristics than was determined from previous tests.

INTRODUCTION

As a continuing part of a current program in airbreathing propulsion, the Lewis Research Center is investigating airframe installation effects on the performance of exhaust nozzle systems appropriate for use at supersonic speeds. In the program, airframe installation effects are being investigated in both wind tunnel and flight tests at off-design subsonic and transonic speeds.

Recent experience has shown that performance of a nozzle system can be appreciably affected by installation on an aircraft, especially at off-design conditions (refs. 1 to 7). With an engine nacelle installation typical of supersonic cruise aircraft, the nacelle may be installed close to the lower surface of a large wing with the nozzle extending downstream of the wing trailing edge. This aft location of the nacelle provides shielding of the inlet by the forward wing surface to minimize angle-of-attack effects and may also provide favorable interference between the nacelle and wing. To investigate the effect of the transonic airframe flow field on nozzle performance for a nacelle of this type, the Lewis Research Center is conducting a flight test program using a modified F-106B aircraft with underwing engine nacelles. The nacelles house J85-GE-13 afterburning turbojet engines. This flight system provides the capability of testing complex nozzles at a larger size than possible in wind tunnels where models are limited to small size to avoid wall interference effects.

The exhaust nozzles reported herein simulated the geometry of a variable-flap ejector (VFE) nozzle operating at off-design subsonic and transonic speeds. With this type of nozzle, the required expansion ratio for efficient operation over a wide range in nozzle pressure ratios and flight speeds is obtained by modulating the position of the variable shroud flaps. At high subsonic speeds, for example, the required exit area will be considerably smaller than that required at supersonic cruise. The flaps may be located at various positions depending upon the flap design, pumping characteristics, and pressure ratio schedule for any particular nozzle.

One intent of this test series was to investigate the effect on boattail drag of moving the nozzle forward underneath the wing by shortening the shroud of the basic nozzle (ref. 8; radius ratio, 0.5; boattail angle, 15°). Shortening the shroud moves the nozzle exit closer to the primary exit. Another configuration was tested where the location underneath the wing was the same as the basic nozzle but the nozzle exit diameter was decreased (less overexpanded) to improve the internal thrust performance. This low-area-ratio nozzle provided a more optimum design for installed operation, where the boattail drag is much less than the isolated value. For this series of tests, nozzle gross thrust coefficients and boattail drag coefficients were obtained. The internal thrusts are compared to tests performed in an altitude-propulsion test facility at the Lewis Research Center (ref. 9). The boattail drag coefficients are compared with the results obtained for the basic nozzle from an earlier series of tests on the F-106 aircraft (ref. 8). Thrust coefficients were obtained by using the turbojet gas generator method of reference 10 and the thrust measuring system described in reference 11. This report also includes more information on the nacelle boundary-layer characteristics. These tests were performed over a Mach number range from 0.6 to 1.3 at nonreheat and reheat power settings.

APPARATUS AND PROCEDURE

Aircraft and Nacelles

The modified F-106B aircraft is shown in flight (fig. 1) with aft-mounted underwing engine nacelles. Installed underneath the right wing is the reference nozzle used to obtain the nacelle drag (ref. 11); a VFE nozzle is shown installed underneath the left wing. This aircraft uses a low, delta-wing design. Figure 2 is a closeup view of the basic VFE nozzle showing how the nozzle is located under the wing. Figure 3 is a closeup view of the shortened nozzle showing the forward location under the wing, and figure 4 is a view from the rear of the same nozzle showing the extreme downward position of the elevon and the elevon cutout area. Figure 5 is a closeup view of the low-area-ratio nozzle in its position under the wing.

A schematic drawing of the aircraft details and nacelle installation and dimensions are shown in reference 8. The aircraft is 20.076 meters (790.4 in.) long and has a 60° sweptback delta-wing planform with a 5.812-meter (228.8-in.) semispan. The wing has an approximate 4-percent-thick NACA 0004-65 airfoil section with a cambered leading edge. The nacelles were mounted to the wing aft lower surface by two attachment links (which were enclosed by strut fairings) on each side of the fuselage at a spanwise distance of 1.863 meters (73.34 in.), or 32.05-percent semispan. Each nacelle houses a J85-GE-13 afterburning turbojet engine; a normal shock (or pitot) inlet with a 6.1° cowl angle was used ahead of the engine. The nacelles included an interface at either end, permitting the testing of various types of inlets and nozzles.

The three fixed-geometry VFE nozzle configurations that were tested are shown in figure 6. All three nozzles had boattail angles of 15° and boattail juncture radius ratios of 0.5. The basic VFE nozzle is one of the same nozzles discussed in reference 8, in which boattail drag coefficients were reported. The second configuration is the shortened VFE nozzle, which has the same dimensions as the basic nozzle except for the ejector shroud length which is 30.48 centimeters (12 in.) shorter. The third nozzle has the same dimensions as the basic nozzle except that the nozzle exit area has been reduced, which increases the boattail area from 54.8 percent of the projected nozzle area A_{β}/A_n to 62.8 percent. This made it necessary to restrict the maximum power setting to minimum reheat to avoid overheating the engine compartment. The basic nozzle and the shortened nozzle with an internal diameter of 42.67 centimeters (16.8 in.) were sized to provide adequate secondary cooling air during maximum reheat operation and were therefore slightly larger than would be required for subsonic cruise at minimum reheat power setting.

Instrumentation

The aircraft was equipped with a digital data system that multiplexed and recorded quasi-static data on magnetic tape (ref. 11). The data system used Scanivalves to measure pressures and had the capability of measuring 578 parameters. A flight-calibrated test boom located on the aircraft nose was used to determine free-stream static and total pressure along with aircraft angle of attack and yaw angle.

The nozzles were instrumented with 12 external static-pressure taps located upstream of the boattail shoulder, with three pressure stations at each of four angular coordinates, as shown in figure 7. The boattails were instrumented with a total of 90 static-pressure orifices located at 10 angular coordinates, with nine axial stations for each angular coordinate. The nine orifices at each angular coordinate were located such that an equal projected area was assigned to each orifice. These orifices were then used to obtain the boattail axial pressure drag coefficient defined as follows:

$$C_{D_\beta} = -\frac{1}{A_n} \sum_{i=1}^{90} C_{p,i} A_i$$

where $C_{p,i}$ is the local boattail pressure coefficient and A_i is the projected area assigned to the i^{th} orifice. The average pressure measured by the eight internal orifices located at the nozzle trailing edge was used as the exit static pressure. This average pressure ratioed to free-stream static was used to indicate if the nozzle was overexpanded or underexpanded.

Nozzle boundary-layer rake instrumentation details are shown in figure 8. Nacelle boundary-layer rake data were obtained at six angular coordinate positions. The three outboard rakes each had six total-pressure tubes and a rake height of 7.62 centimeters (3.0 in.); these are a duplicate of the rakes reported in reference 8. Three rakes each of which had eight total-pressure tubes were added to the inboard side of the nozzle. The rake height was increased to 12.8 centimeters (5.04 in.) because in reference 8 the boundary layer was found to be somewhat thicker than 7.62 centimeters at Mach numbers near 0.95. Two of the rakes were located differently than in reference 8 to get a better idea of the circumferential variation of the boundary layer. The two new positions were located at 217^o and 255^o. The static-pressure orifice used to calculate each tube Mach number was located near the base of each rake flush with the nozzle surface.

Procedure

Tests were conducted at flight Mach numbers from 0.5 to 1.3 and Reynolds numbers

that varied from 8.5×10^6 per meter (2.6×10^6/ft) at Mach 0.6 to 14×10^6 per meter (4.4×10^6/ft) at Mach 1.3. The aircraft was flown at a nominal altitude - Mach number profile, as shown in figure 9. This altitude profile resulted in the nominal angles of attack and trim elevon deflections shown in figure 10.

A schematic drawing of the engine installation in the nacelle is shown in figure 11, along with the nacelle station designations. The J-85 engine had a variable-area primary nozzle that modulated with changes in power setting. This modulation changes the location of the primary exit plane and convergence angle as shown in figure 11(b). A more detailed description of the J-85 and the calibrations of the engines to determine the airflow conditions entering the VFE nozzles are found in reference 10. Secondary cooling air to the nozzles was determined from in-flight calibrations (ref. 11) of the flow control valves using the calibrated pumping characteristics of a reference nozzle (ref. 9). Tests were conducted at the nozzle pressure ratio schedules for the three VFE nozzles, as shown by figure 12. The basic nozzle and the low-area-ratio nozzle were tested on the left nacelle, while the shortened nozzle was tested on the right nacelle. A thrust measuring system described in reference 11 was used to determine the gross thrust of the installed nozzles. The gross thrust of the nozzle is equal to the thrust measured by the load cell plus the calibrated nacelle tare force coefficient as described in reference 11.

RESULTS AND DISCUSSION

Nozzle Thrust Characteristics

Flight tests were conducted to determine the thrust characteristics of the three VFE nozzles operating at reheat and nonreheat power settings with various amounts of secondary airflow. Figure 13 shows a comparison of the thrust characteristics for the three nozzles tested in (military) nonreheat and minimum reheat power settings. Thrust data in maximum reheat power were taken with the shortened nozzle only and, therefore, were not used for comparison purposes. The minimum reheat power setting provides a primary- to nozzle-external-diameter ratio typical of that required for an advanced propulsion system operating at subsonic cruise.

The nonreheat (military) power setting resulted in ejector- to primary-exit-nominal-effective-diameter ratios $d_9/d_{e,8}$ of 1.450, 1.415, and 1.330 or ejector nozzle-external-diameter-to-primary-exit-effective-diameter ratios $d_n/d_{e,8}$ of 2.17, 2.11, and 2.18 for basic, shortened, and low-area-ratio VFE nozzles, respectively. With a minimum reheat power setting, the resulting ejector- to primary-exit-diameter ratios were 1.300, 1.285, and 1.180 or $d_n/d_{e,8}$ of 1.93, 1.91, and 1.93 for the same three respective nozzles.

The low-area-ratio nozzle produced the highest gross thrust coefficient of the three nozzles tested for both minimum reheat and nonreheat (military) power settings. This was due to an improvement of the internal performance, which results because the decreased exit diameter provides an ejector- to primary-nozzle-exit-area ratio which more nearly matches the ideal expansion ratio. The installed boattail drag coefficient is near zero, so that boattail area causes very little thrust loss. The shortened nozzle had the next highest thrust except between Mach 0.96 and 0.99 for nonreheat (military) power setting and between 0.93 and 1.10 for minimum reheat (see ref. 9; fig. 25, basic ejector against shortened ejector). The reason for the poorer thrust near Mach 1.0 was because the drag rise occurred at a lower Mach number for the shortened nozzle than for the basic ejector.

The gross thrust coefficient for the installed basic ejector nozzle and a comparison of the internal performance coefficient with the quiescent data in reference 9 for nonreheat (military) and minimum reheat power settings are shown in figure 14. The flight data were taken over a range of secondary corrected weight flows of 0.03 to 0.06, and the nominal values are presented in the lower half of the figure. In the upper half of each figure the flight data were interpolated at specific values of corrected secondary flow ratio. For this comparison with static data, the boattail drag in flight was determined from the measured pressure drag, and an estimated skin friction drag was used. The boattail drag and skin friction drag were added together to obtain the total external drag D_{ext}. The internal performance in flight agreed well with the static data, especially at Mach numbers from 0.8 to 1.0 for the nonreheat condition shown in figure 14(a). The largest difference was at Mach 0.69, where the flight internal performance coefficient fell 0.0175 below the curve predicted by the static calibration with 0.04 corrected secondary-weight-flow ratio.

The flight results and a comparison with the static calibration for minimum reheat power setting are shown in figure 14(b). Again, the results show that the flight data are very close to the static calibration from Mach 0.8 to 1.0, but are much lower at Mach 0.69 than with the nonreheat power setting.

The flight results for the shortened nozzle and a comparison with the static calibration of internal performance coefficient are shown in figure 15 for nonreheat (military), minimum reheat, and maximum reheat settings. Results are presented in a manner similar to that of figure 14. There is fairly good agreement between the flight data and the static calibration up to Mach 0.9 for the nonreheat power setting. Above Mach 0.9 the flight data are generally higher and exhibit quite a lot of scatter. With a minimum reheat power setting, the flight data agreed well with the static calibration only for Mach 0.8 to 1.0 with 0.04 corrected secondary-weight-flow ratio; the data were lower below Mach 0.8 and higher at the higher Mach numbers. For 0.06 and 0.08 corrected secondary-weight-flow ratios, all the flight data were higher except at Mach 0.6 where the flight data were very close to the static calibration. In the maximum reheat power

setting, no comparison was attempted because no static data were taken at ejector nozzle-exit- to primary-nozzle-diameter ratios smaller than 1.18.

The flight data for the low-area-ratio ejector nozzle is shown in figure 16 for nonreheat (military) and minimum reheat primary power settings. This ejector was not tested in the static altitude facility. This nozzle proved to have the highest gross thrust coefficient of the three tested because of the better internal performance even with the penalty of a slightly higher boattail drag. Typical values of thrust coefficient in minimum reheat at Mach 0.9 with a 0.04 corrected secondary weight flow ratio are 0.978 for the low-area-ratio nozzle, 0.930 for the basic nozzle, and 0.953 for the shortened nozzle. With the favorable interference effect obtained with this nozzle, the peak performance occurred at Mach 0.95 and resulted in a thrust coefficient of 0.998.

Boattail Drag

The ratios of nozzle boattail pressure drag to ideal primary thrust for the three nozzles with the various power settings are shown in figure 17. All three nozzles had essentially the same ratio of drag to ideal primary thrust from Mach numbers of 0.6 to 0.8, and the basic and shortened nozzles were about the same up to Mach 0.9. The shortened nozzle drag rise started at Mach 0.9; the basic and low-area-ratio nozzles exhibited a sudden drop in drag at Mach 0.9 and reached a minimum at Mach 0.95, and then the drag rise occurred. The sudden drop in drag exhibited by the other two nozzles did not occur for the shortened nozzle because the 30.48-centimeter (12-in.), more forward location of the shortened nozzle placed the boattail in the lower pressure region and some of the boattail had separated flow. The low-area-ratio nozzle with the largest boattail area (62.8 percent of A_n against 54.8 for the basic nozzle) had a slightly higher drag ratio from Mach 0.8 to 0.95 and at supersonic Mach numbers than the basic nozzle in nonreheat (military) and minimum reheat power settings.

The boattail drag coefficients (fig. 18) had essentially the same characteristics and relative levels as did the boattail- to ideal-primary-thrust ratios since the ideal primary thrust is approximately the same for each nozzle at each power setting. The basic nozzle curves are from results reported in reference 8, which also presents the boattail pressure distributions for the 10 rows of static-pressure orifices. It should be noted that the drag rise occurs at a lower Mach number for the shortened nozzle at all three power settings than for the basic or low-area-ratio nozzles due to its more forward location underneath the wing. The shortened nozzle had a higher supersonic drag coefficient than the basic nozzle but lower than the low-area-ratio nozzle, which had the largest boattail area.

The boattail pressure distribution for the shortened nozzle is presented in figure 19 for maximum reheat power. The overall level of the pressure coefficients is lower than

the data of reference 8. Also there were some regions of flow separation for some of the upper rows, where the boattail is closest to the lower surface of the wing. The pressure distribution for the low-area-ratio nozzle is presented in figure 20 but only up to Mach 1.085 and for minimum reheat instead of maximum reheat power setting since no data were obtained in maximum reheat. It can be seen that with the low-area-ratio nozzle which has the boattail beyond the trailing edge of the wing there was no separation of the flow over the boattail.

Nacelle Boundary Layer

Earlier results of the static-pressure measurements on the nozzle boattails showed there was quite a circumferential variation of static pressure, especially on the forward part of the boattail (ref. 8). The same trend is seen from the test results reported herein and shown in figures 19 and 20. Test data were obtained in order to calculate and study the boundary-layer characteristics of the flow approaching the nozzle boattail. Previous measurements of the nacelle boundary layer reported in reference 8 showed the boundary layer was quite thick and distorted, with regions of possible separation. To further investigate this circumferential variation and distortion, three rows of tufts were attached to the outboard side of the right nacelle with a reference nozzle installed, and the heights of the rakes were increased on the inboard side.

The momentum thickness and displacement thickness were calculated by integrating the boundary-layer profile out to the tube which read the highest total pressure. The momentum thickness for each rake for a Mach number range of 0.7 to 1.3 is shown in figure 21(a) for the capture mass flow ratio that would be required for a military power setting and a 0.04 corrected secondary-weight-flow ratio. Shown also in this figure are the values that would be obtained using flatplate theory with a 1/7 power profile. Results from the boundary-layer calculations show both the displacement and momentum thicknesses to be greater than would be calculated theoretically except for the rakes at 45° and 217°. The data agreed closely with those reported in reference 8 for those rake positions that were the same (45°, 105°, 165°, and 255°). The two new positions (217° and 285°) show that the circumferential variations are even greater than those first measured (ref. 8) and that at 217° the momentum thickness is less than predicted by flatplate theory. The momentum thickness at the 285° position is also quite small and close to a 1/7 profile. The ratio of displacement thickness to momentum thickness is shown in figure 21(b) for the six rakes. As to be expected, the rake at 217° shows a very high exponent (greater than 11), which would be required to give lower momentum thickness values than a 1/7 profile.

Tufts were attached on the outboard side of the nacelle, and motion pictures were

taken at various Mach numbers to give a visual indication of the boundary-layer flow over the nacelle. A number of frames taken from the motion-picture film at a Mach number of 0.9 are shown in figure 22. The tufts in all three rows beyond the point of maximum nacelle cross-sectional area showed quite a bit of oscillation from side to side. The fourth tuft (labeled A in fig. 22) from the back in the bottom row seemed to be the worst, with about 120° total movement. The tufts were installed only on the outboard side since it was more convenient to photograph, although the inboard side showed the most distorted profiles, as can be seen in the individual velocity profiles in figure 23.

The individual velocity profiles for the six rakes are shown for various Mach numbers from 0.78 to 1.3. Some of the other important parameters are listed for each rake, such as the capture mass flow ratio, rake maximum velocity to free-stream velocity ratio, maximum total-pressure to free-stream total-pressure ratio, and momentum thickness to nacelle maximum diameter ratio. It can be seen that the only location where the boundary-layer thickness exceeded the shorter rake height of 7.62 centimeters (3.0 in.; $x/d_n = 0.12$) was at 255°. At Mach 0.95 all the rakes show their highest value of momentum thickness, and some have quite distorted profiles.

SUMMARY OF RESULTS

To further investigate airframe installation effects on variable-flap ejector nozzles at subsonic and transonic speeds, a flight test investigation was conducted using a modified F-106B aircraft with underwing engine nacelles. From earlier tests (ref. 8), it was found that the boattail drag coefficient was significantly reduced at transonic flight Mach numbers for an underwing installation. With this fact known, a low-area-ratio nozzle which has a larger boattail area was tested to determine the overall installation effect. The decrease in exit diameter resulted in a smaller ejector nozzle- to primary-exit-diameter ratio, which resulted in an improved internal performance coefficient. To determine if nozzle location has a significant effect on the boattail drag characteristics, a shortened nozzle configuration was tested. Also, additional data were taken to further investigate the viscous flow field around the nozzle. The nozzles were investigated over a Mach number range from 0.6 to 1.3. Using the basic nozzle configuration from reference 8 as a reference for comparison, the following results were obtained:

1. The nozzle gross thrust coefficient was improved significantly by reducing the ratio of ejector exit area to primary nozzle area. Reducing the exit area changed the area ratio from 1.69 to 1.39 and increased the gross thrust coefficient from 0.930 to 0.978 at a Mach number of 0.9 with 0.04-percent corrected secondary-weight-flow ratio. This increased the boattail area, but the boattail drag was very small compared to the nozzle thrust for this installation. Therefore, the reason for this gain in performance was almost entirely due to the increased internal performance.

2. Shortening the nozzle, which effectively moved the nozzle boattail 0.48 nozzle diameter forward underneath the wing, caused the boattail drag rise to occur earlier by 0.02 Mach number. Also, the boattail drag coefficient was higher between Mach 0.9 and 0.95, and no longer exhibited a large drop at Mach 0.95. This change in drag coefficient caused the nozzle gross thrust coefficient to peak at Mach 0.9 instead of Mach 0.95 for the minimum reheat condition.

3. A series of tests with measurements taken to determine the boundary-layer characteristics immediately upstream of the nozzle boattail showed that, for small variations in circumferential location, there were even greater circumferential variations in nacelle boundary-layer characteristics than was determined from previous tests (ref. 8).

Lewis Research Center,
National Aeronautics and Space Administration,
Cleveland, Ohio, October 12, 1971,
764-74.

APPENDIX - SYMBOLS

A_n	cross-sectional area of nozzle cylindrical section, 3166.9 cm^2 (490.9 $in.^2$)
A_β	projected area of nozzle boattail
C_{D_β}	axial boattail pressure drag coefficient in direction of nozzle axis, (Axial force)/$q_0 A_n$
C_p	pressure coefficient, $(p - p_0)/q_0$
D	drag in direction parallel to nozzle axis
d	diameter
F	axial thrust
h	pressure altitude
M	Mach number
m_0	mass flow at free-stream conditions through an area equal to nacelle inlet capture area
m_1	mass flow captured by nacelle inlet
N	exponent in boundary-layer velocity equation, $V/V_{bl} = (z/\delta)^{1/N}$
P	total pressure
p	static pressure
q	dynamic pressure, $0.7 p_0 M_0^2$
R	radius
r	boattail juncture radius of curvature
V	velocity
x	nozzle axial distance coordinate
z	radial distance from nozzle external surface
α_0	aircraft angle of attack
α_p	primary nozzle convergence angle
δ	boundary-layer thickness
δ^*	boundary-layer displacement thickness
δ^{**}	boundary-layer momentum thickness
δ_e	elevon deflection angle; +down, -up
τ	ratio of secondary to primary total temperatures at station 8

φ	nozzle angular coordinate
ω	ratio of secondary to primary weight flows at station 8
$\omega\sqrt{\tau}$	corrected secondary-weight-flow ratio

Subscripts:

bl	boundary layer
e	effective
ext	external
f	external surface friction
ip	ideal primary
max	maximum parameter measured or calculated in boundary layer
n	nozzle
p	primary
s	secondary
0	free-stream or flight condition
1-9	nacelle and nozzle stations (fig. 11)

REFERENCES

1. Greathouse, William K.: Blending Propulsion with Airframe. Space/Aeronautics, vol. 50, no. 6, Nov. 1968, pp. 59-68.

2. Corson, Blake W., Jr.; and Runckel, Jack F.: Exploratory Studies of Aircraft Afterbody and Exhaust-Nozzle Interaction. NASA TM X-1925, 1969.

3. Runckel, Jack F.: Aerodynamic Interference Between Exhaust System and Airframe. Aerodynamic Interference. AGARD-CP-71-71, Jan. 1971.

4. Schnell, W. C.; and Migdal, D.: An Experimental Evaluation of Exhaust Nozzle/ Airframe Interference. J. Aircraft, vol. 7, no. 5, Sept.-Oct. 1970, pp. 396-400.

5. Blaha, Bernard J.; and Mikkelson, Daniel C.: Wind Tunnel Investigation of Airframe Installation Effects on Underwing Engine Nacelles at Mach Numbers from 0.56 to 1.46. NASA TM X-1683, 1968.

6. Blaha, Bernard J.; Mikkelson, Daniel C.; and Harrington, Douglas E.: Wind Tunnel Investigation of Installation Effects on Underwing Supersonic Cruise Exhaust Nozzles at Transonic Speeds. NASA TM X-52604, 1969.

7. Blaha, Bernard J.: Effect of Underwing Nacelle Shape and Location on Boattail Drag and Wing Pressures at Mach Numbers From 0.56 to 1.46. NASA TM X-1979, 1970.

8. Mikkelson, Daniel C.; and Head, Verlon L.: Flight Investigation of Airframe Installation Effects on a Variable Flap Ejector Nozzle of an Underwing Engine Nacelle at Mach Numbers From 0.5 to 1.3. NASA TM X-2010, 1970.

9. Samanich, Nick E.; and Huntley, Sidney C.: Thrust and Pumping Characteristics of Cylindrical Ejectors Using Afterburning Turbojet Gas Generator. NASA TM X-52565, 1969.

10. Antl, Robert J.; and Burley, Richard R.: Steady-State Airflow and Afterburning Performance Characteristics of Four J85-GE-13 Turbojet Engines. NASA TM X-1742, 1969.

11. Groth, Harold W.; Samanich, Nick E.; and Blumenthal, Philip Z.: Inflight Thrust Measuring System for Underwing Nacelles Installed on a Modified F-106 Aircraft. NASA TM X-2356, 1971.

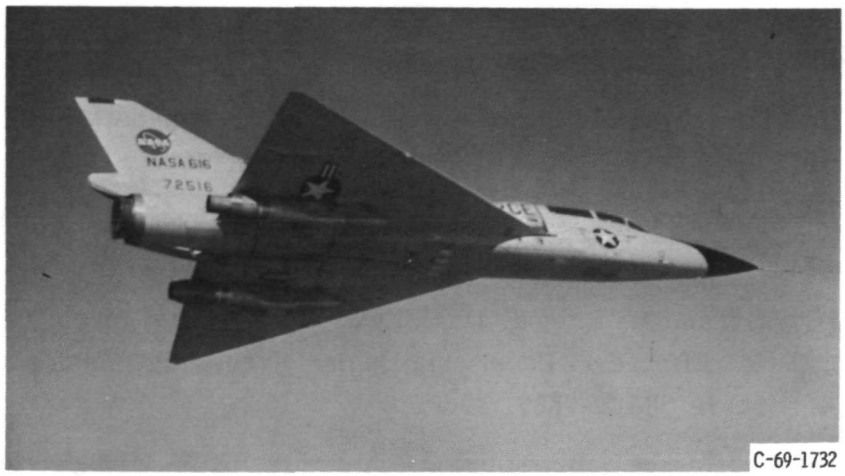

Figure 1. - Modified F-106B aircraft in flight, showing underwing installation of nozzles.

Figure 2. - Basic variable-flap ejector nozzle located under trailing edge of wing.

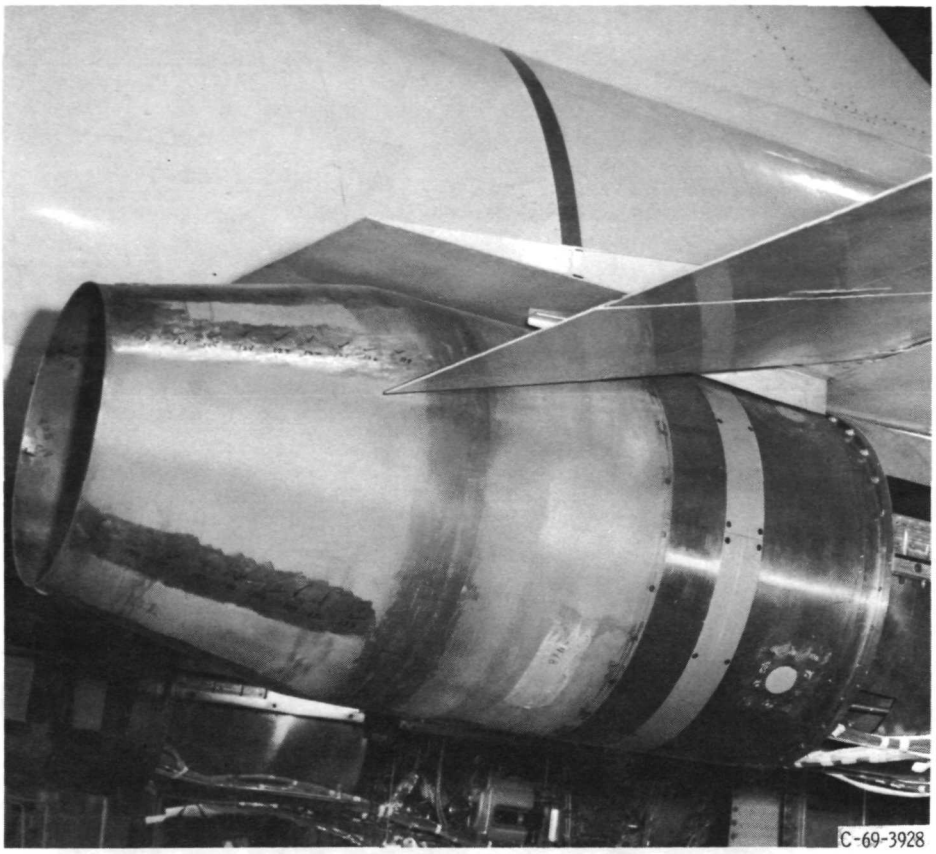

Figure 3. - Shortened variable-flap ejector nozzle located under trailing edge of wing.

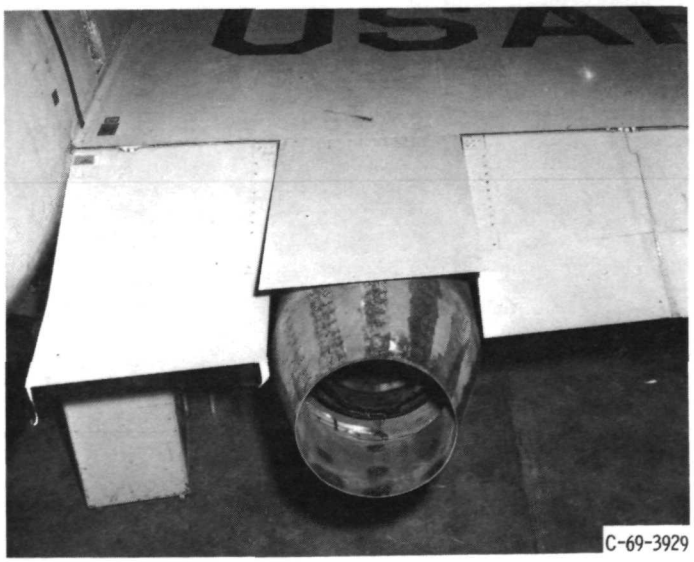

Figure 4. - Shortened variable-flap ejector nozzle showing elevon cutout area with elevons deflected down.

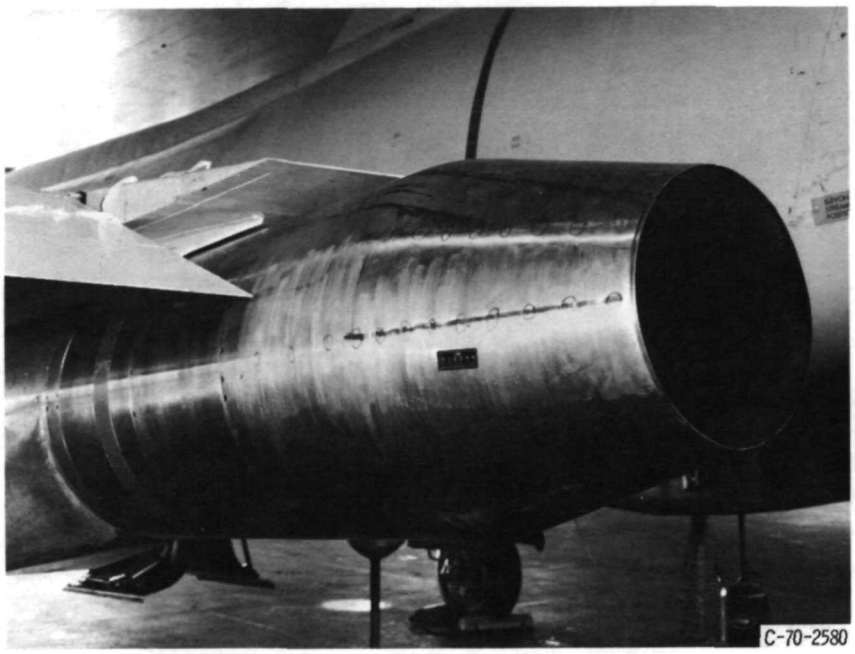

Figure 5. - Low-area-ratio variable-flap ejector nozzle located under trailing edge of wing with elevons deflected down.

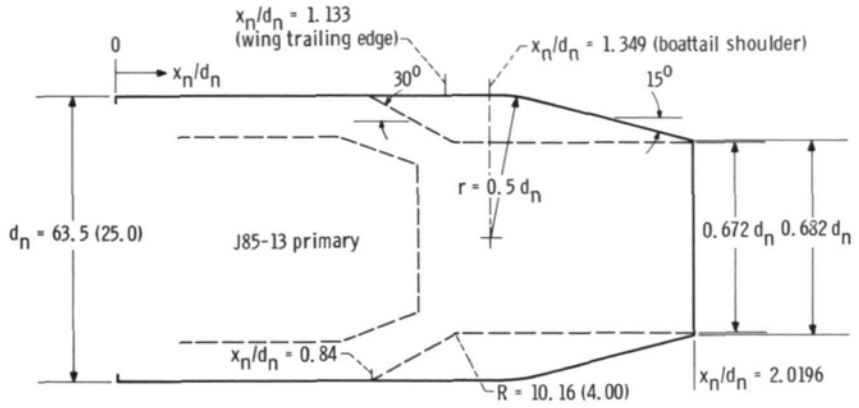

(a) Basic nozzle.

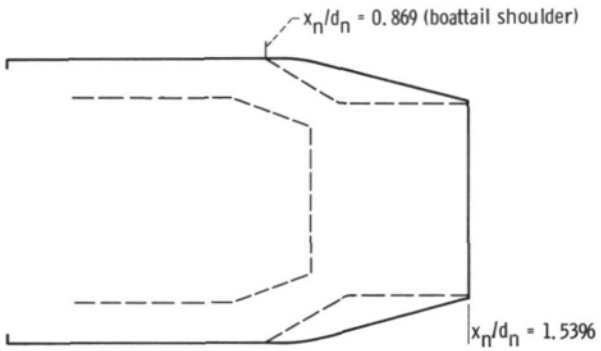

(b) Shortened nozzle

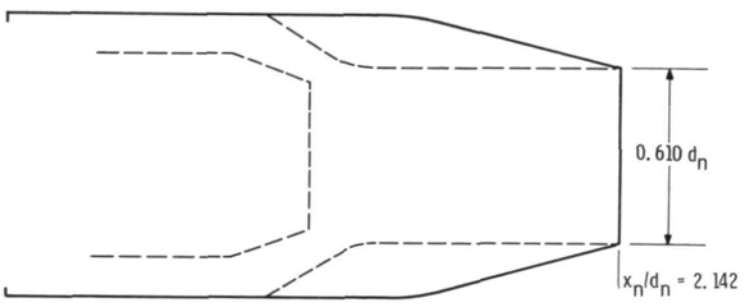

(c) Low-area-ratio nozzle.

Figure 6. - Details of variable-flap ejector nozzle geometry. Shortened nozzle and low-area-ratio nozzle are the same as basic nozzle except as shown. (Dimensions are in cm (in.).)

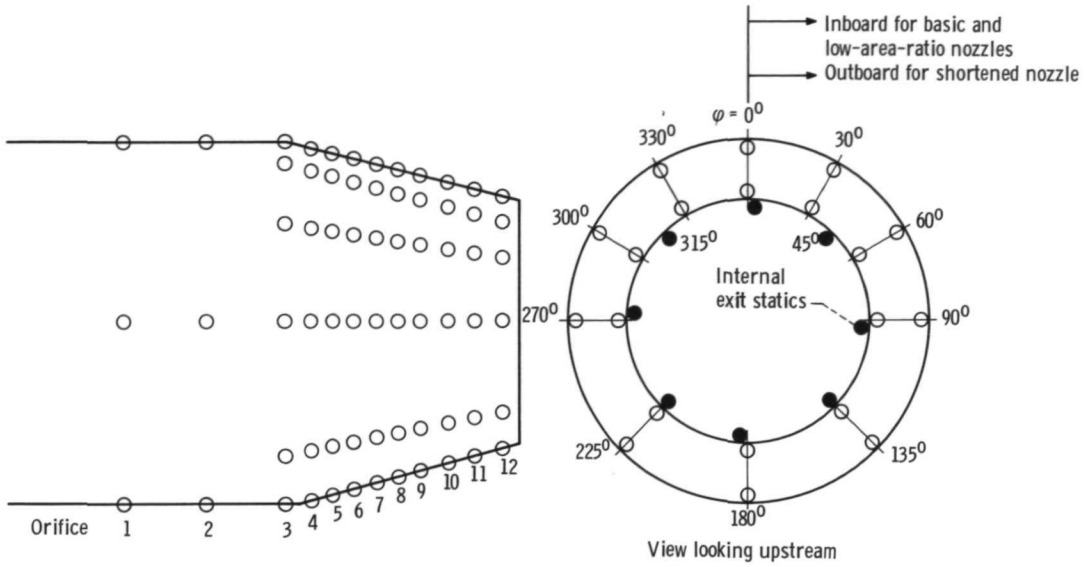

Orifice location on nozzle	Orifice station	Basic nozzle	Short nozzle	Low-area-ratio nozzle	Nozzle angular coordinate, φ, deg
		Nondimensional position coordinate, x_n/d_n			
Forebody	1	0.935	0.500	1.020	0, 90, 180, 270
	2	1.155	.700	1.180	
	3	1.375	.900	1.340	
Boattail	4	1.435	1.020	1.440	0, 30, 60, 90, 135, 180, 225, 270, 300, 330
	5	1.500	1.080	1.514	
	6	1.559	1.140	1.586	
	7	1.620	1.203	1.658	
	8	1.683	1.270	1.735	
	9	1.749	1.338	1.816	
	10	1.819	1.411	1.902	
	11	1.891	1.488	1.993	
	12	1.968	1.540	2.092	
Internal exit statics	--	2.000	1.120	2.102	0, 45, 90, 135, 180, 225, 270, 315

Figure 7. - Nozzle static-pressure instrumentation.

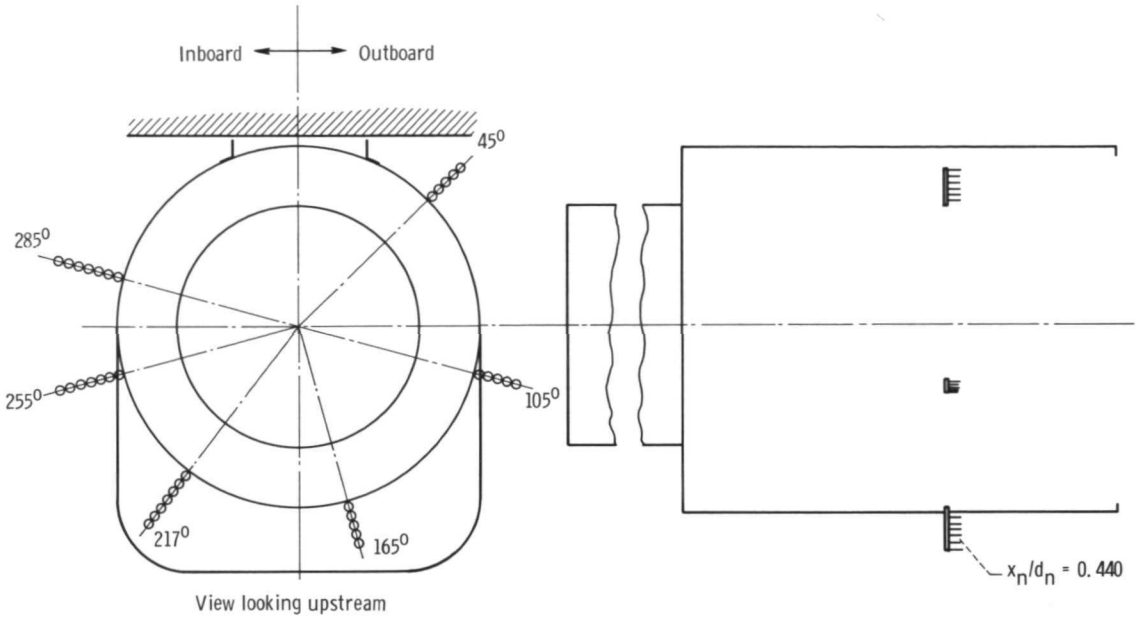

(a) Boundary-layer rake locations.

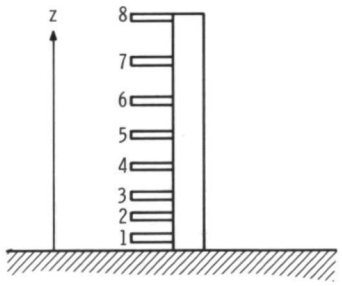

Tube	Inboard rakes	Outboard rakes
	z/d_n	
1	0.0056	0.0060
2	.0168	.0172
3	.0336	.0344
4	.0560	.0568
5	.0840	.0848
6	.1176	.1200
7	.1538	------
8	.2016	------

(b) Boundary-layer rake dimensions.

Figure 8. - Details of boundary-layer instrumentation.

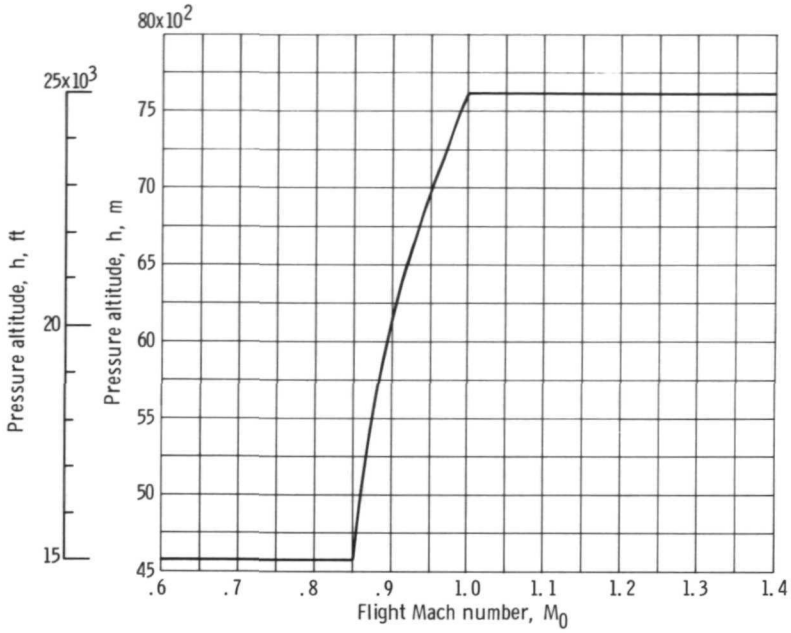

Figure 9. - Nominal flight test altitude - Mach number profile.

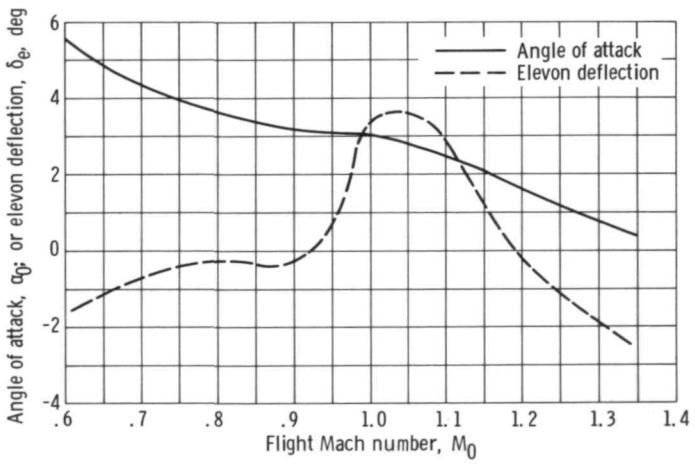

Figure 10. - Nominal angle of attack and elevon deflection with nacelles installed.

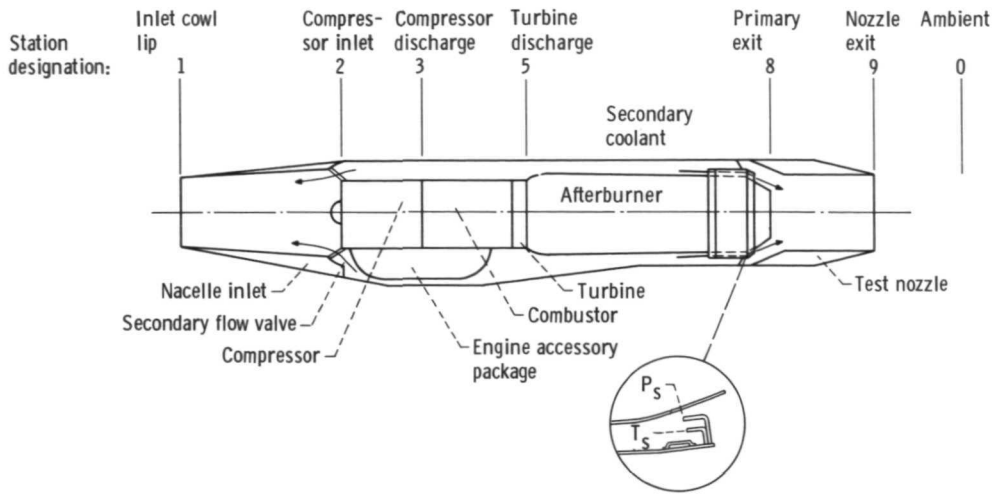

(a) Engine installation and station designation.

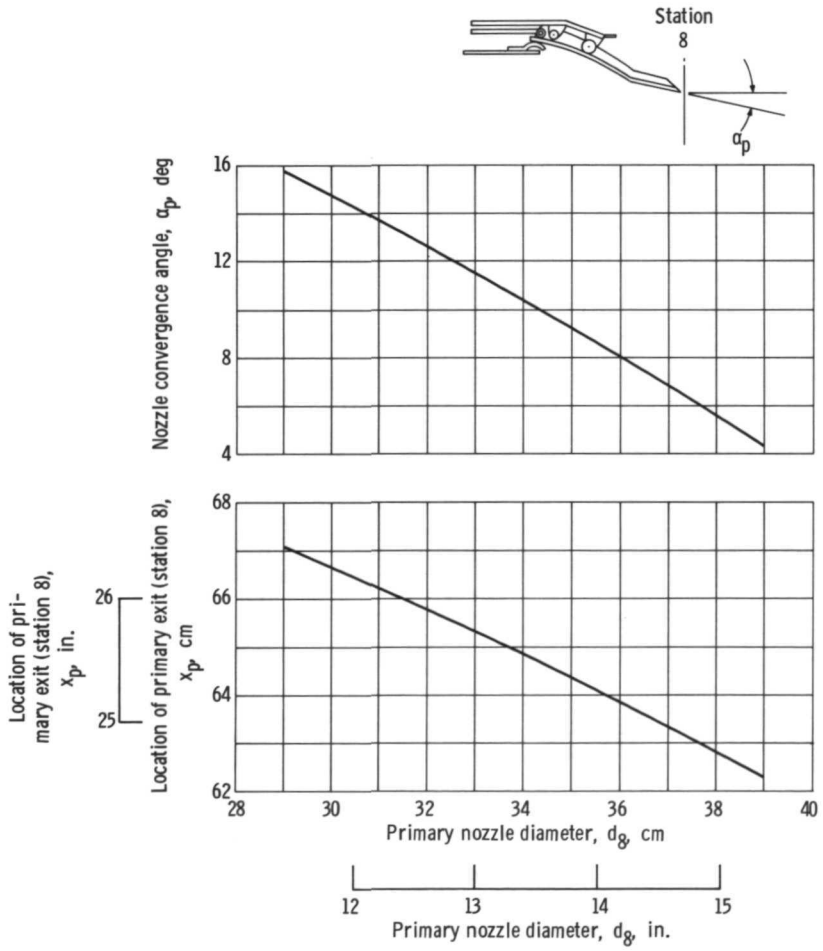

(b) Location of primary nozzle exit and convergence angle.

Figure 11. - Schematic of engine installation and details of primary nozzle.

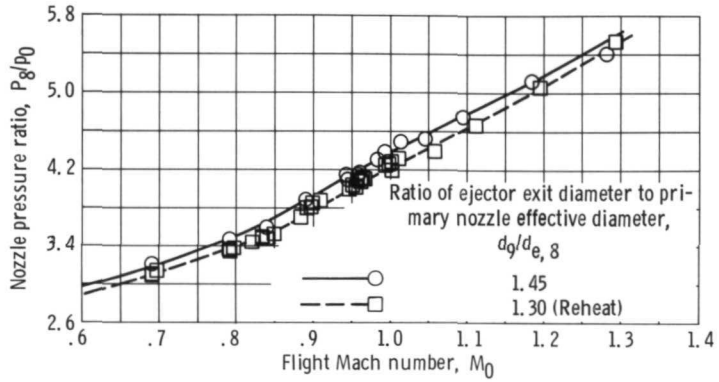

(a) Basic nozzle.

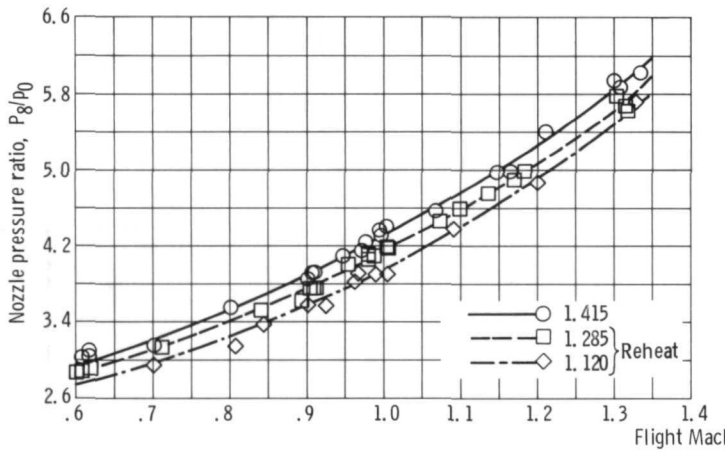

(b) Shortened nozzle.

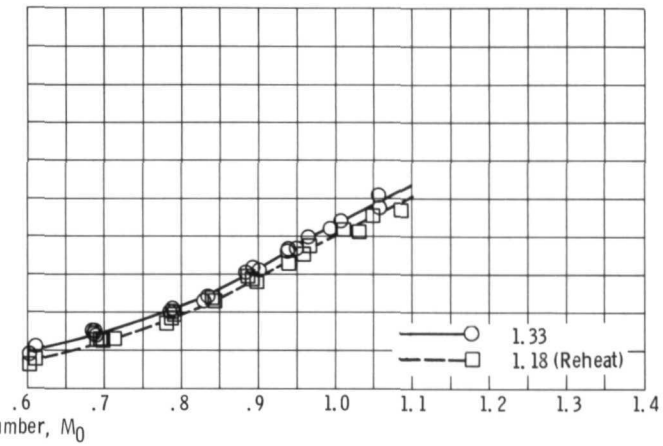

(c) Low-area-ratio nozzle.

Figure 12. - Nozzle pressure ratio schedules.

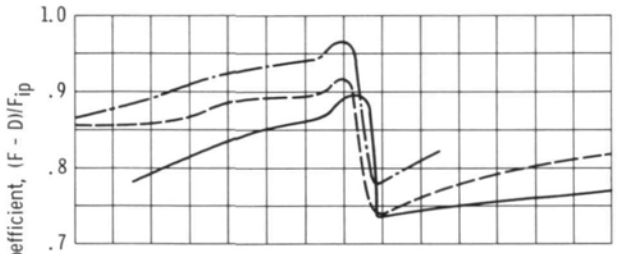

(a) Nonreheat (military) power setting.

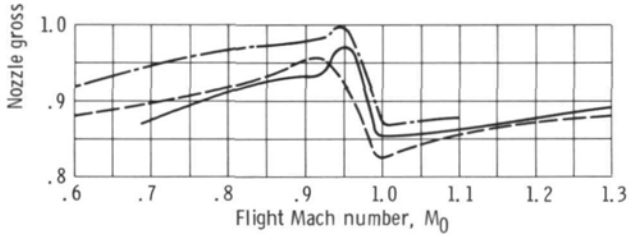

(b) Minimum reheat power setting.

Nozzle gross thrust coefficient, $(F - D)/F_{ip}$

Nozzle	Ratio of ejector exit diameter to primary nozzle effective diameter, $d_9/d_{e,8}$	Corrected secondary weight-flow ratio, $\omega\sqrt{\tau}$
Basic	1.450	0.040
Shortened	1.415	.045
Low area ratio	1.330	.056
Basic	1.300	0.04
Shortened	1.285	
Low area ratio	1.180	

Figure 13. - Comparison of nozzle gross thrust coefficients from flight data.

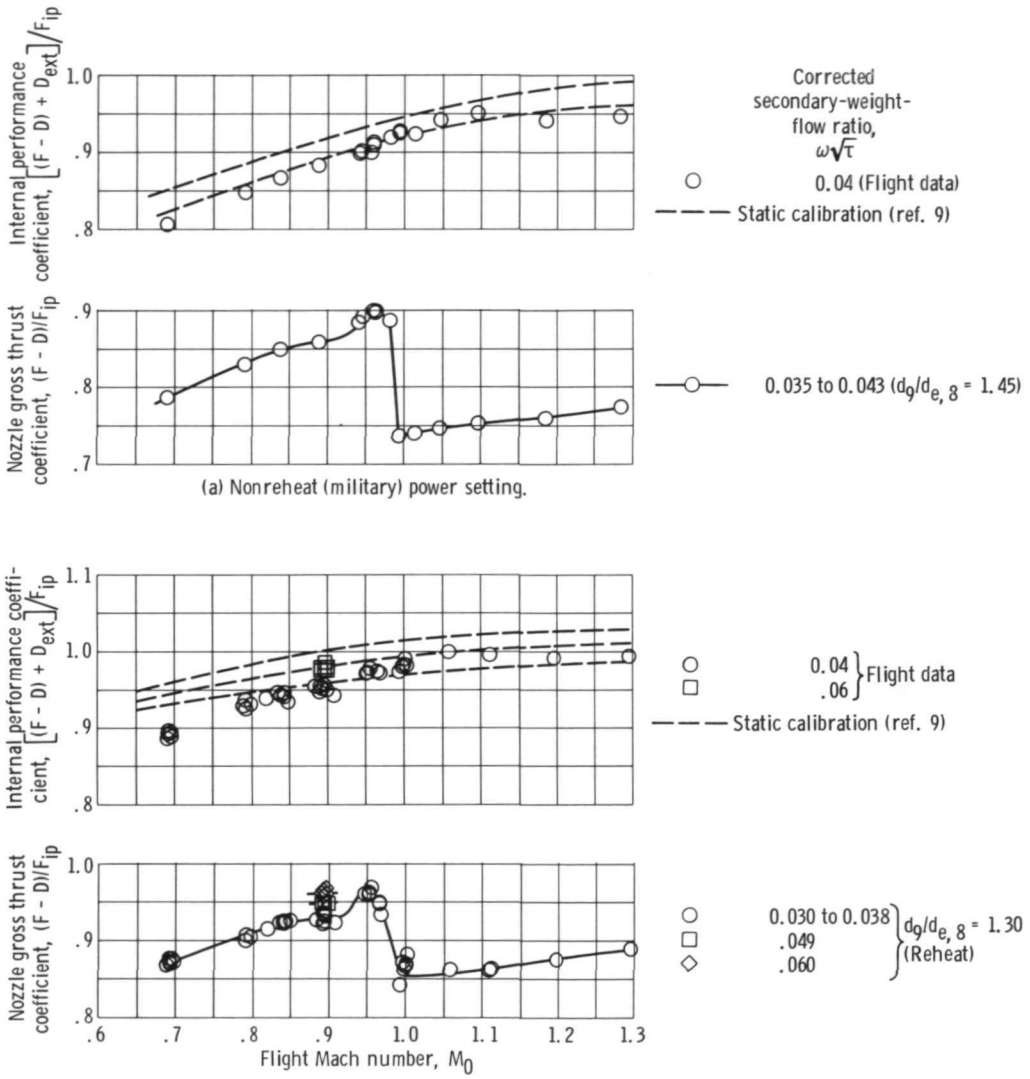

(a) Nonreheat (military) power setting.

(b) Minimum reheat power setting.

Figure 14. - Basic variable-flap ejector nozzle performance.

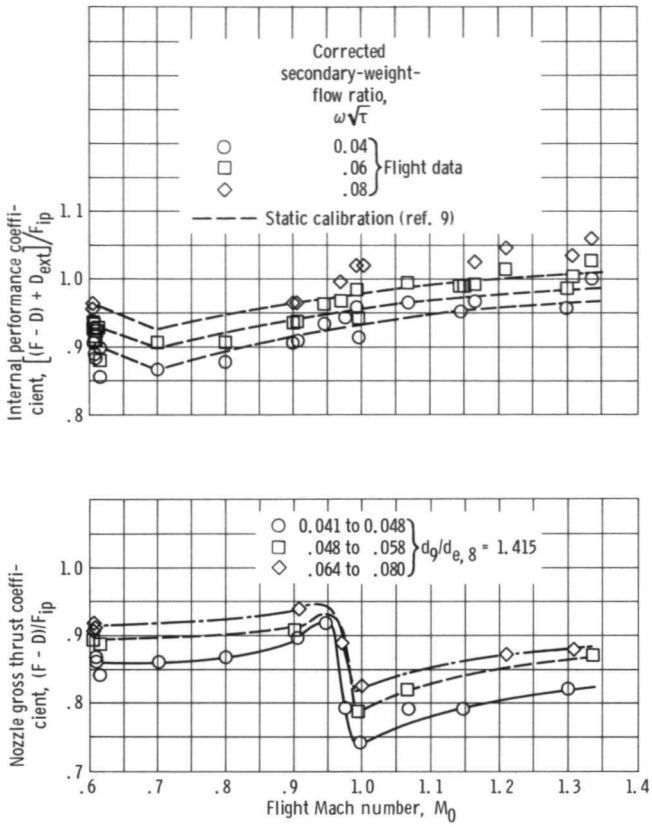

(a) Nonreheat (military) power setting.

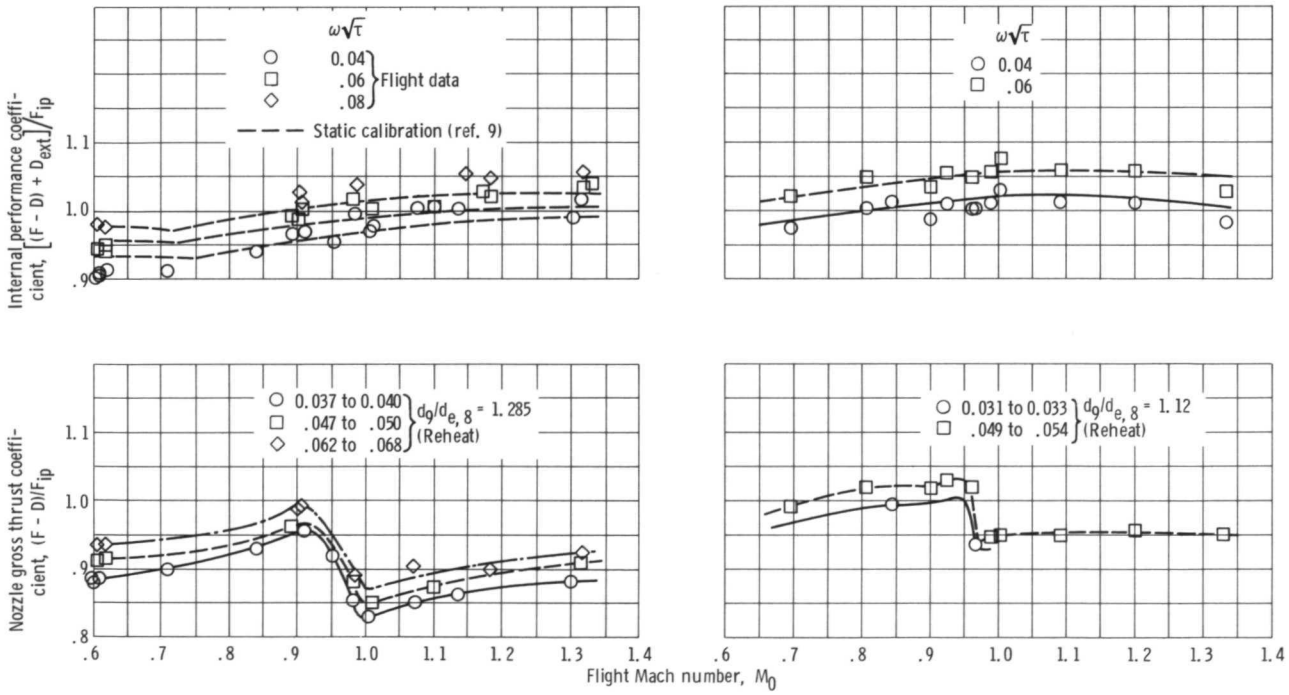

(b) Minimum reheat power setting.

(c) Maximum reheat power setting.

Figure 15. - Shortened variable-flap ejector nozzle performance.

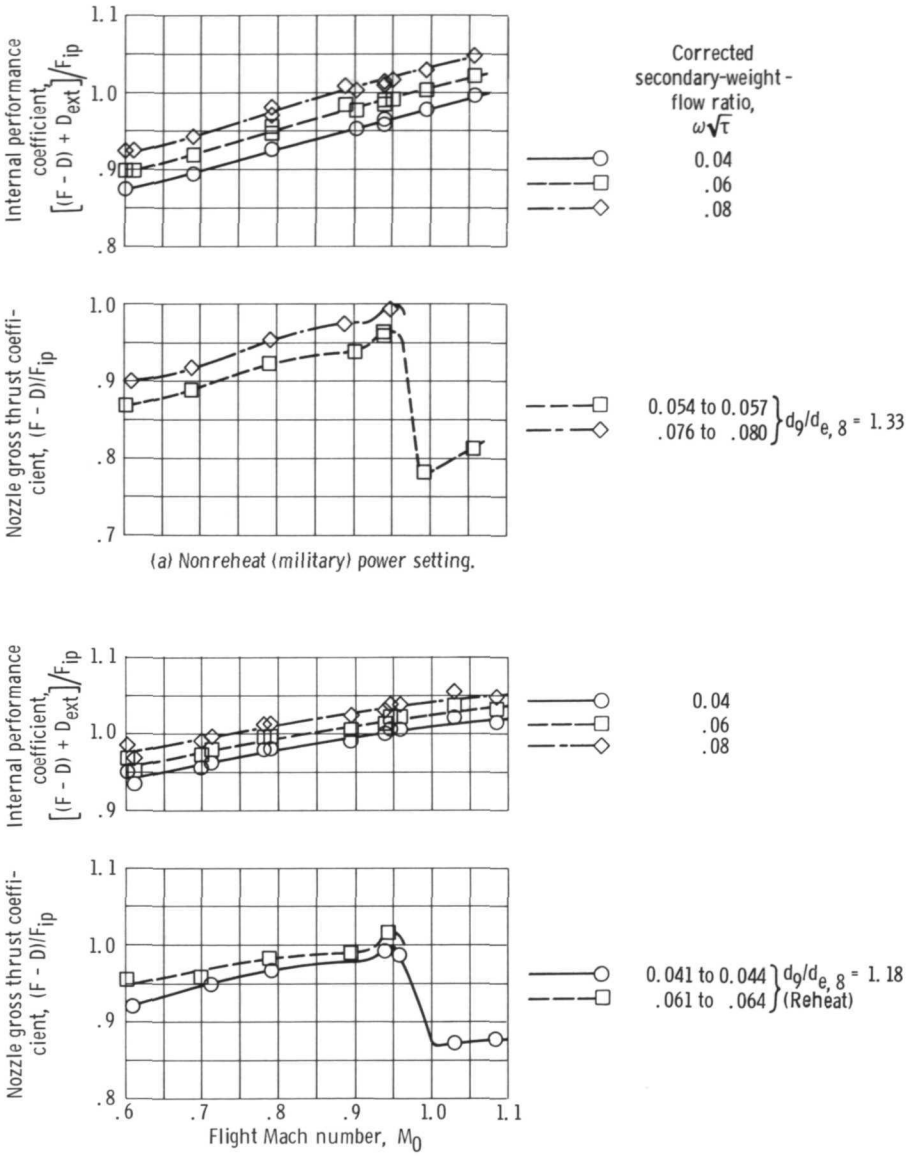

(a) Nonreheat (military) power setting.

(b) Minimum reheat power setting.

Figure 16. - Low-area-ratio variable-flap ejector nozzle performance.

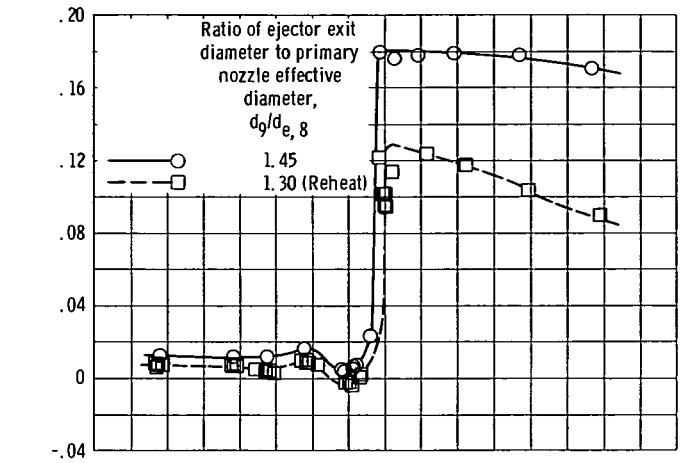

(a) Basic nozzle.

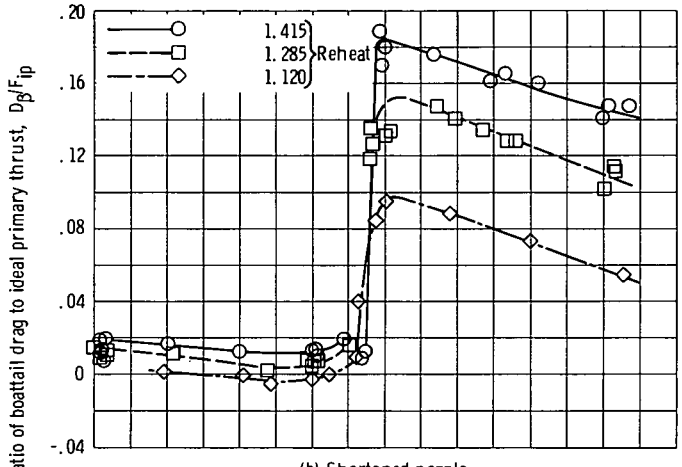

(b) Shortened nozzle.

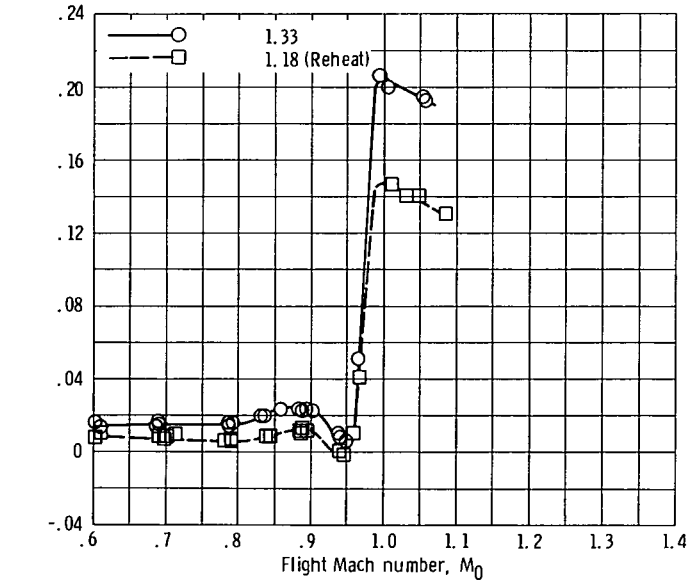

(c) Low-area-ratio nozzle.

Figure 17. - Ratio of nozzle boattail drag to ideal primary thrust.

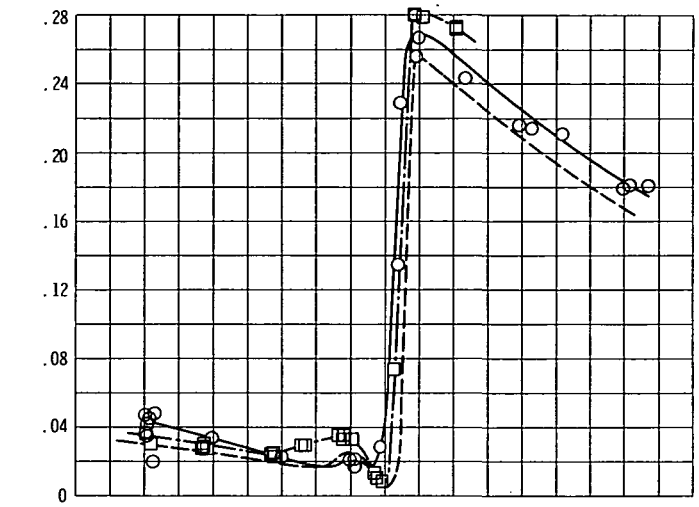

(a) Nonreheat (military) power setting.

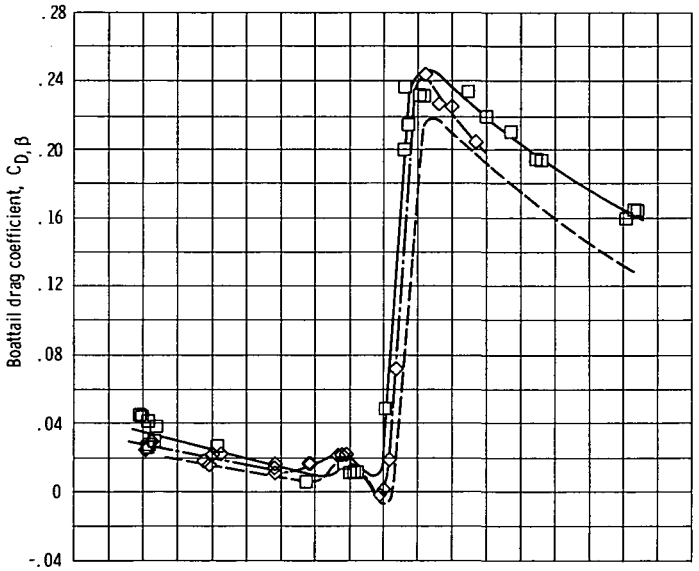

(b) Minimum reheat power setting.

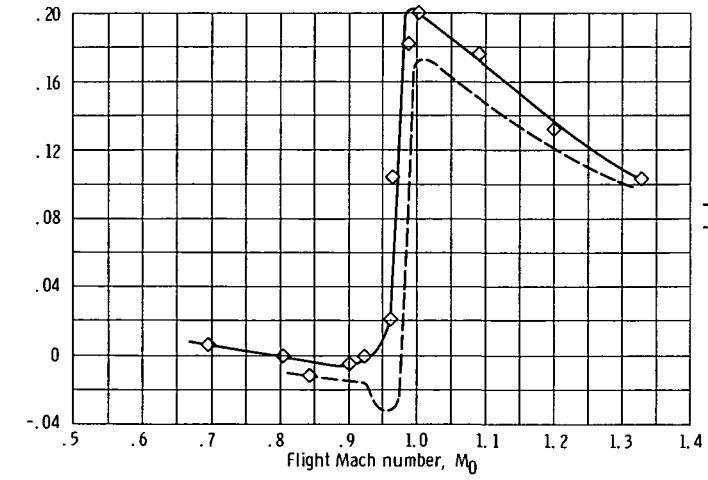

(c) Maximum reheat power setting.

Nozzle	Ratio of ejector exit diameter to primary nozzle effective diameter, $d_9/d_{e,8}$	Corrected secondary-weight-flow ratio, $\omega\sqrt{\tau}$
Basic (ref. 8)	1.450	0.04
Shortened	1.415	0.041 to 0.08
Low area ratio	1.330	.045 to .08
Basic (ref. 8)	1.300	0.04
Shortened	1.285	0.037 to 0.068
Low area ratio	1.180	.042 to .064
Basic (ref. 8)	1.14	0.065
Shortened	1.12	0.031 to 0.054

Figure 18. - Comparison of variable-flap ejector boattail drag coefficients.

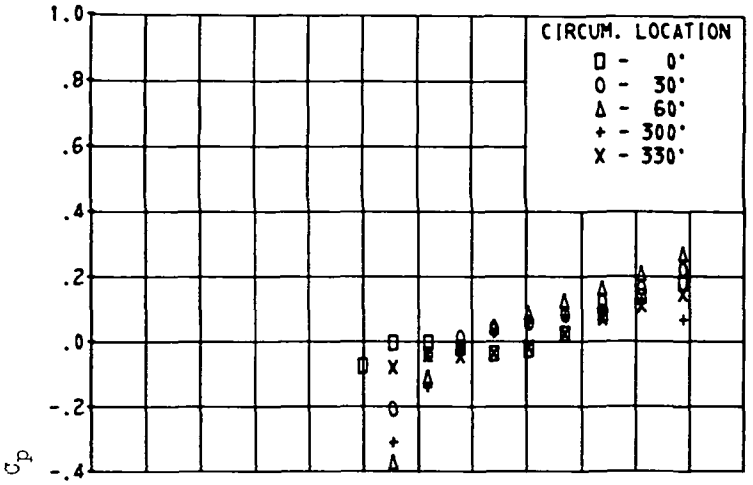

(a-1) Upper half.

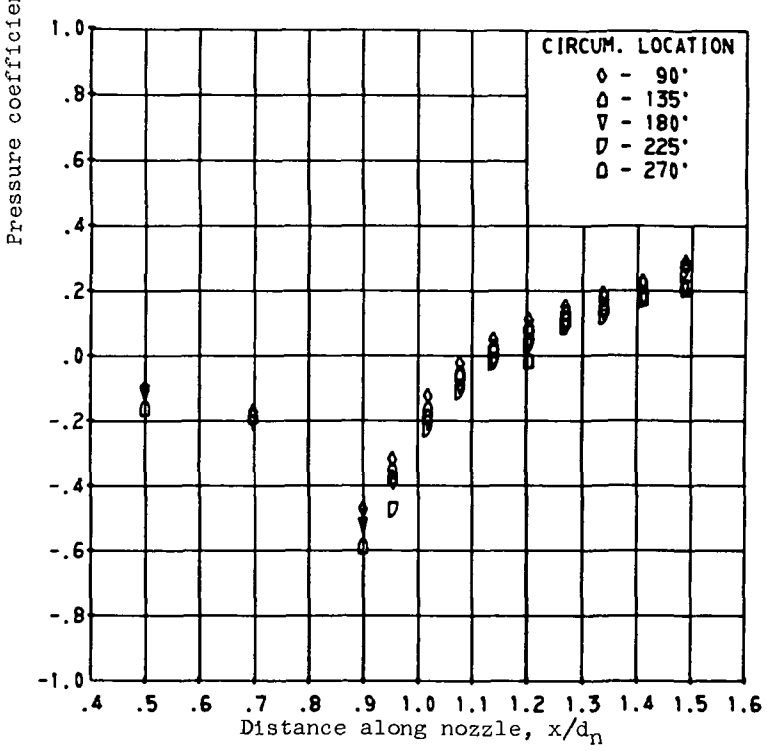

(a-2) Lower half.

(a) $M_0 = 0.806$; $d_9/d_8 = 1.10$; $\omega\sqrt{\tau} = 0.049$.

Figure 19. - Shortened variable-flap ejector nozzle boattail pressure distributions, for several values of flight Mach number M_0, ratio of ejector exit diameter to primary nozzle exit diameter d_9/d_8, and corrected secondary-weight-flow ratio $\omega\sqrt{\tau}$. Maximum reheat power setting.

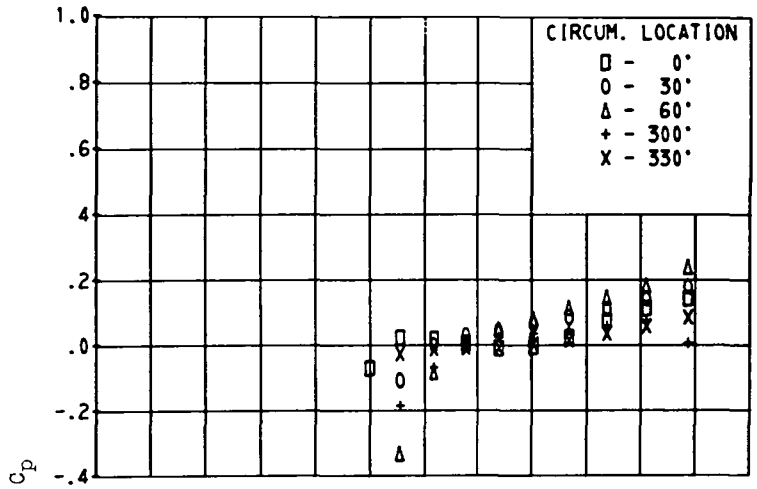

(b-1) Upper half.

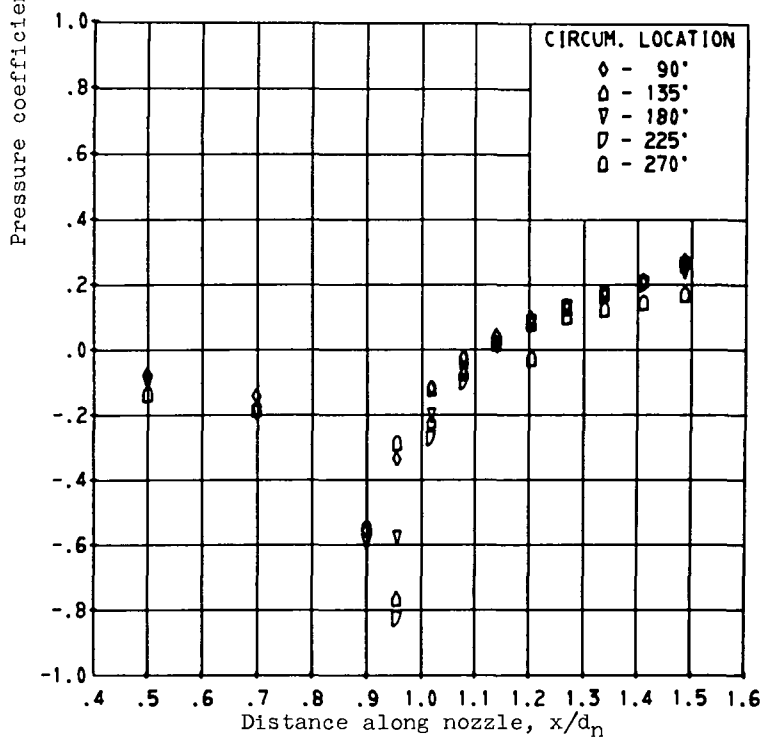

(b-2) Lower half.

(b) $M_0 = 0.901$; $d_9/d_8 = 1.120$; $\omega\sqrt{\tau} = 0.054$.

Figure 19. - Continued.

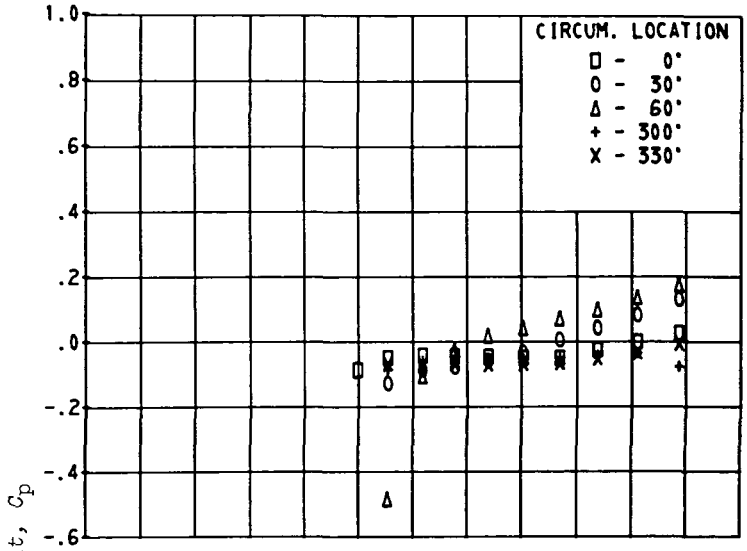

(c-1) Upper half.

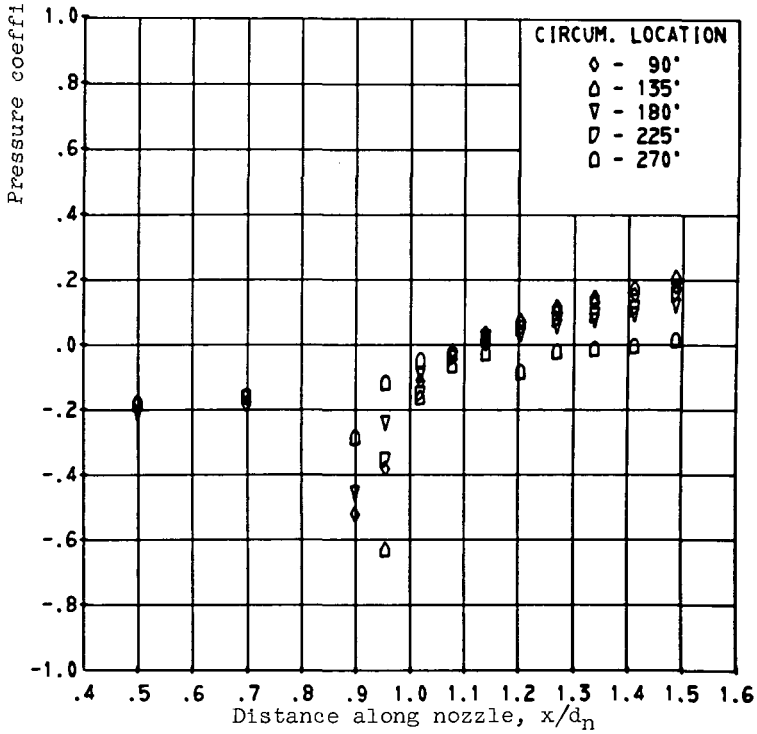

(c-2) Lower half.

(c) $M_0 = 0.962$; $d_9/d_8 = 1.131$; $\omega\sqrt{\tau} = 0.053$.

Figure 19. - Continued.

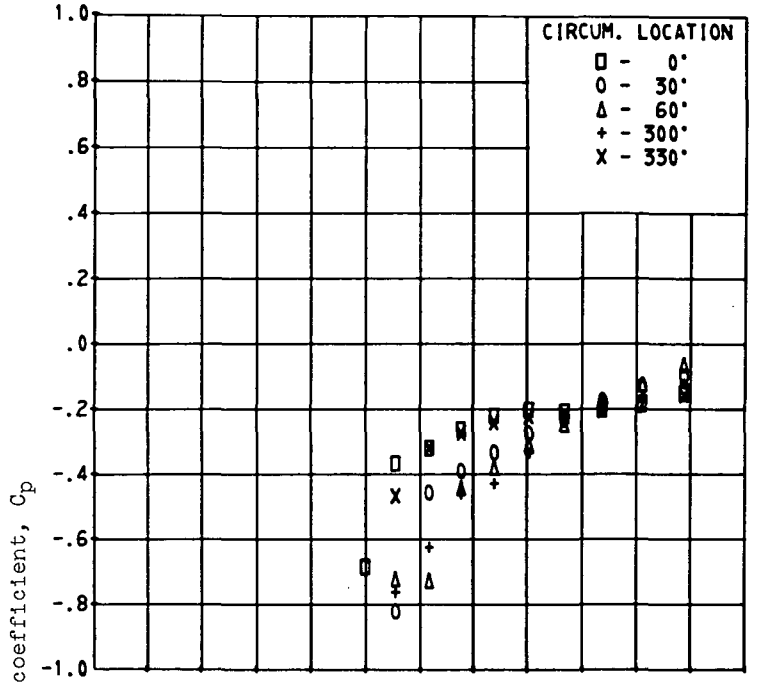

(d-1) Upper half.

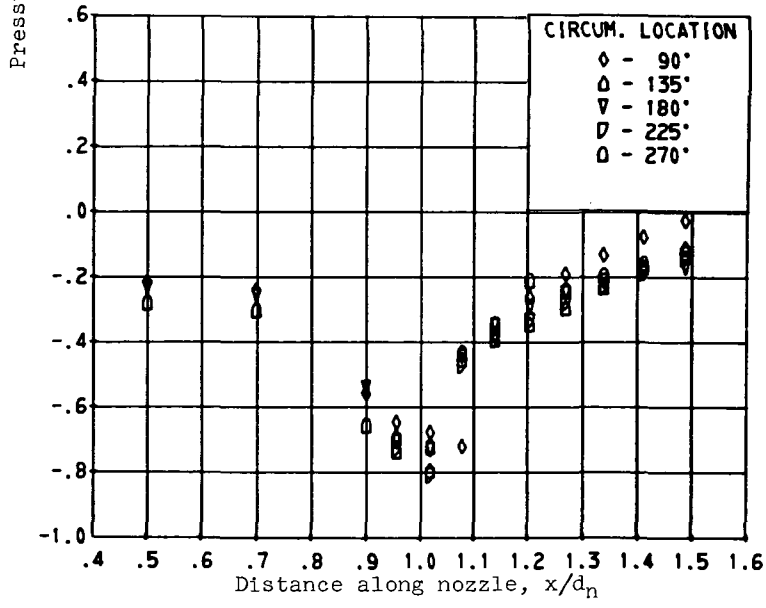

(d-2) Lower half.

(d) $M_O = 1.004$; $d_9/d_8 = 1.102$; $\omega\sqrt{\tau} = 0.048$.

Figure 19. - Continued.

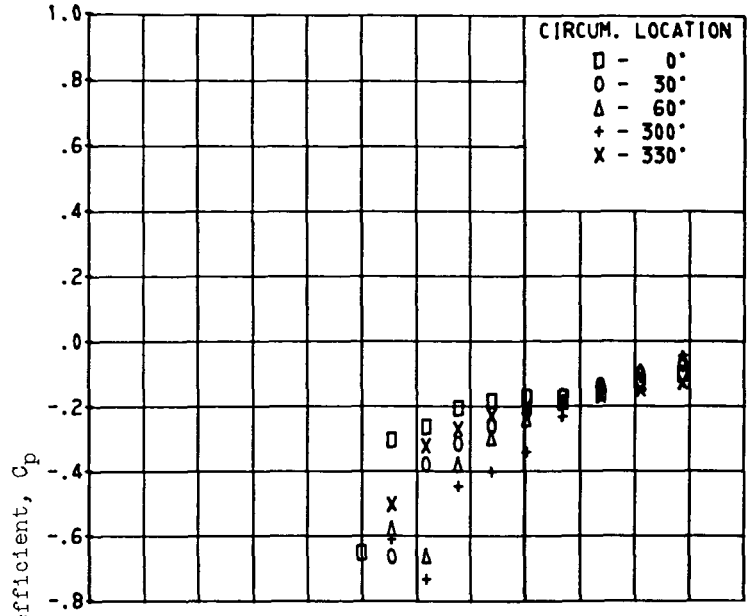

(e-1) Upper half.

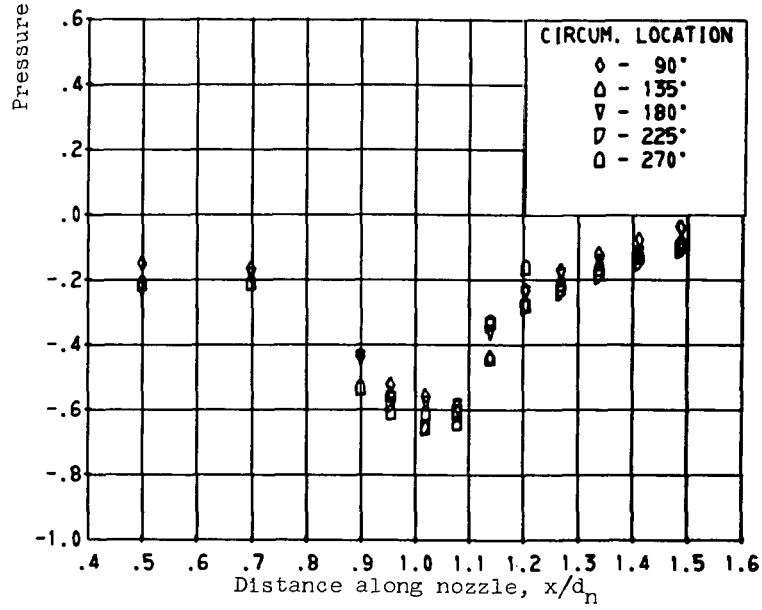

(e-2) Lower half.

(e) $M_0 = 1.092$; $d_9/d_8 = 1.121$; $\omega\sqrt{\tau} = 0.053$.

Figure 19. - Continued.

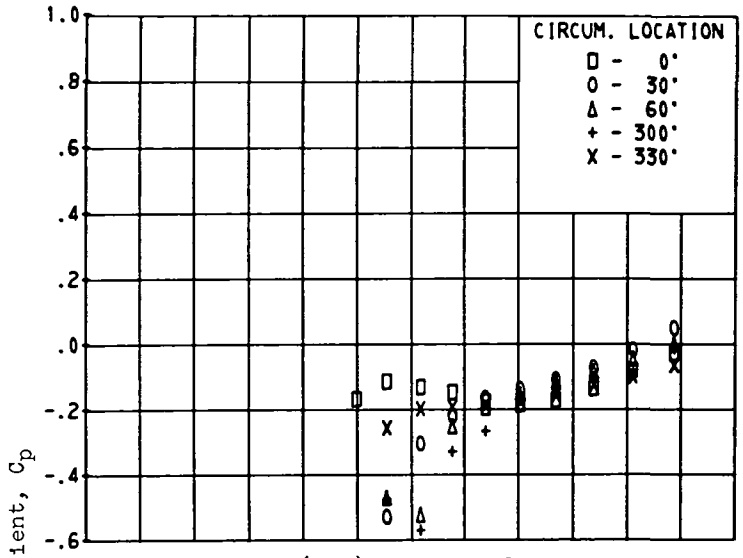

(f-1) Upper half.

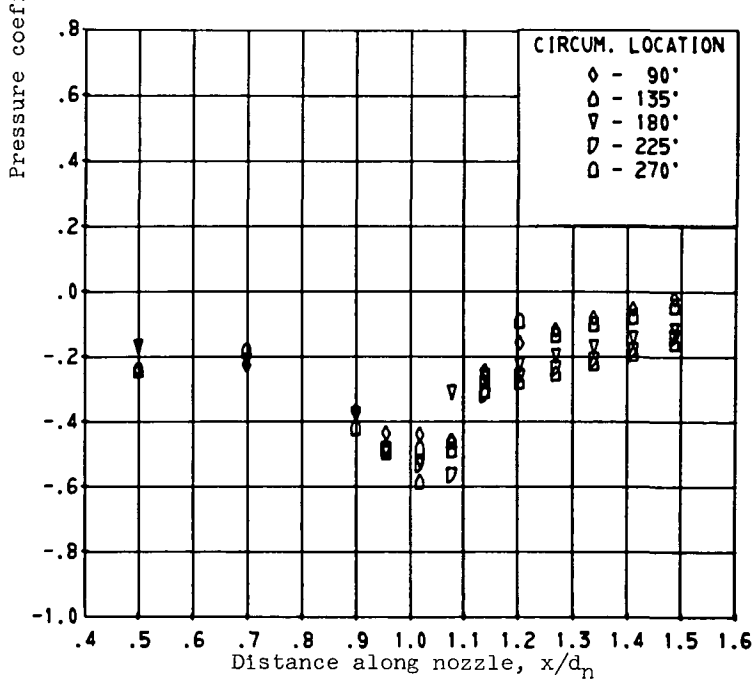

(f-2) Lower half.

(f) $M_0 = 1.201$; $d_9/d_8 = 1.121$; $\omega\sqrt{\tau} = 0.051$.

Figure 19. - Concluded.

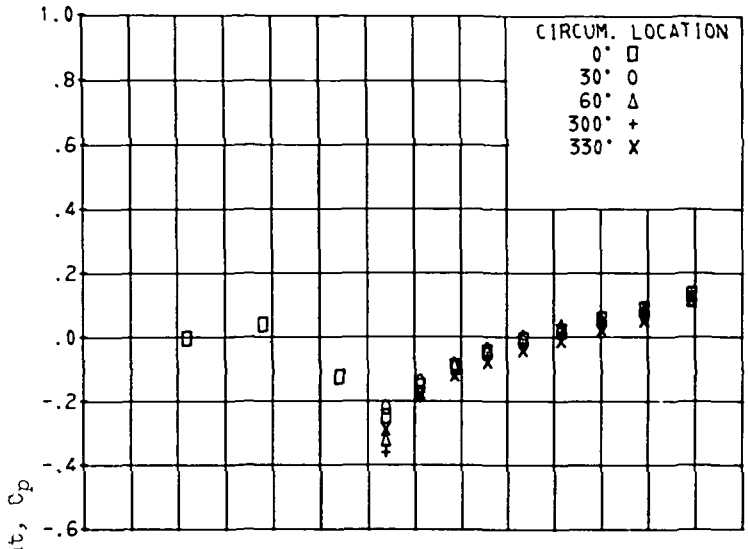

(a-1) Upper half.

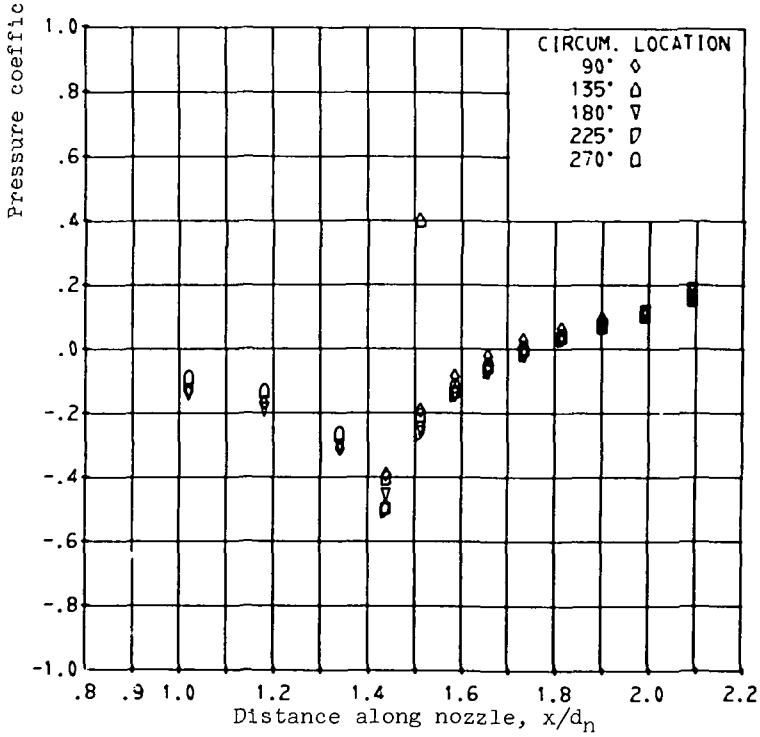

(a-2) Lower half.

(a) $M_0 = 0.610$; $d_9/d_8 = 1.19$; $\omega\sqrt{\tau} = 0.0441$.

Figure 20. - Low-area-ratio variable-flap ejector nozzle boattail pressure distributions, for several values of flight Mach number M_0, ratio of ejector exit diameter to primary nozzle exit diameter d_9/d_8, and corrected secondary-weight-flow ratio $\omega\sqrt{\tau}$. Minimum reheat power setting.

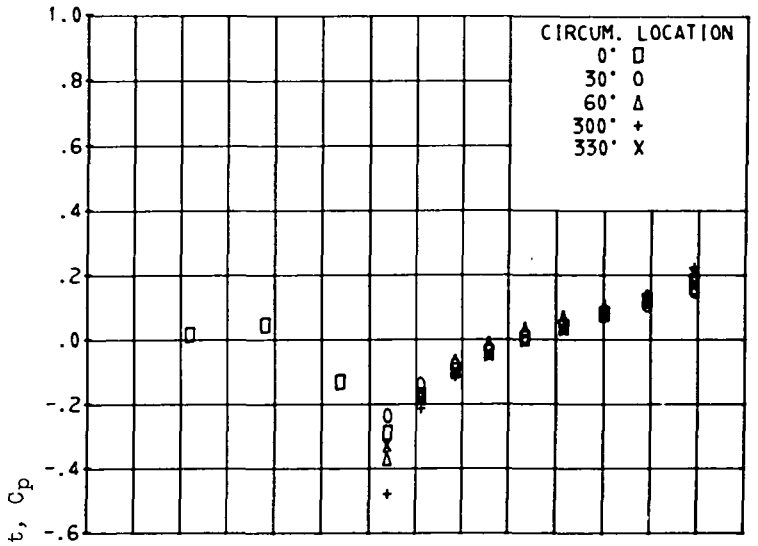

(b-1) Upper half.

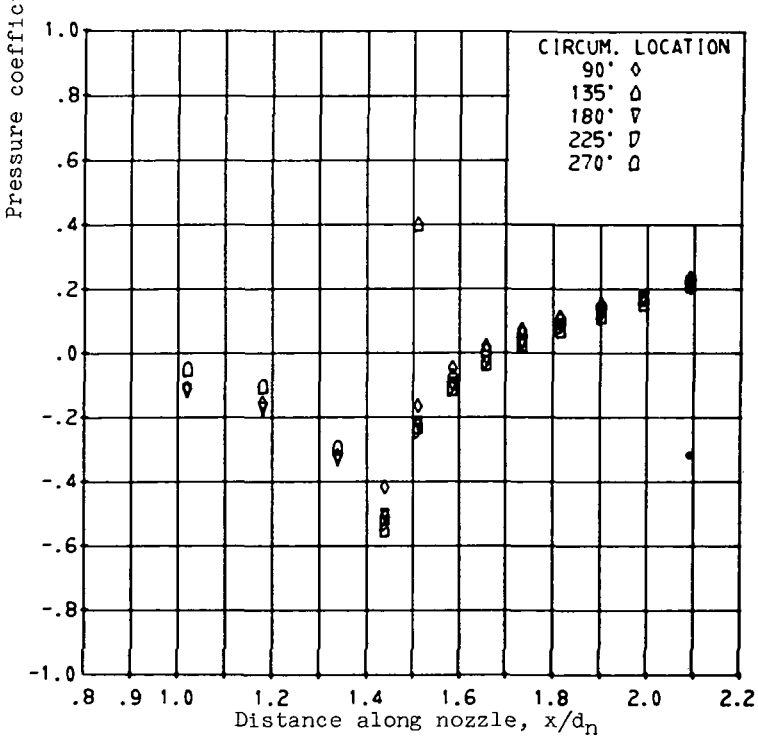

(b-2) Lower half.

(b) $M_0 = 0.792$; $d_9/d_8 = 1.17$; $\omega\sqrt{\tau} = 0.0424$.

Figure 20. - Continued.

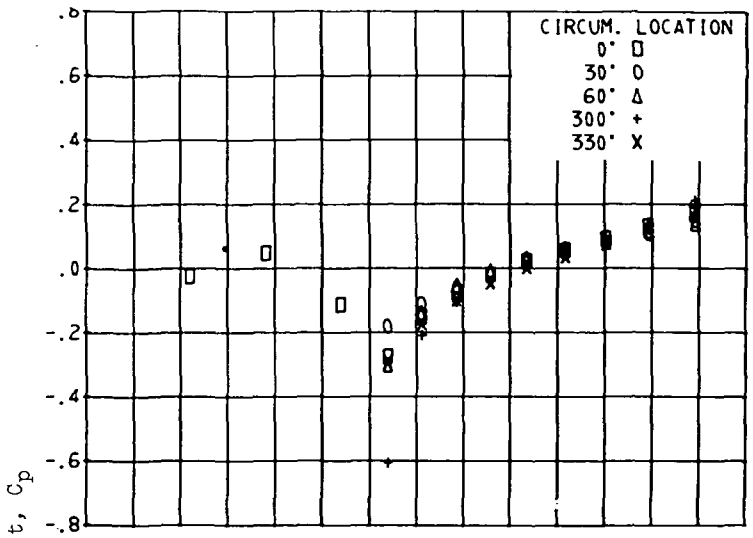

(c-1) Upper half.

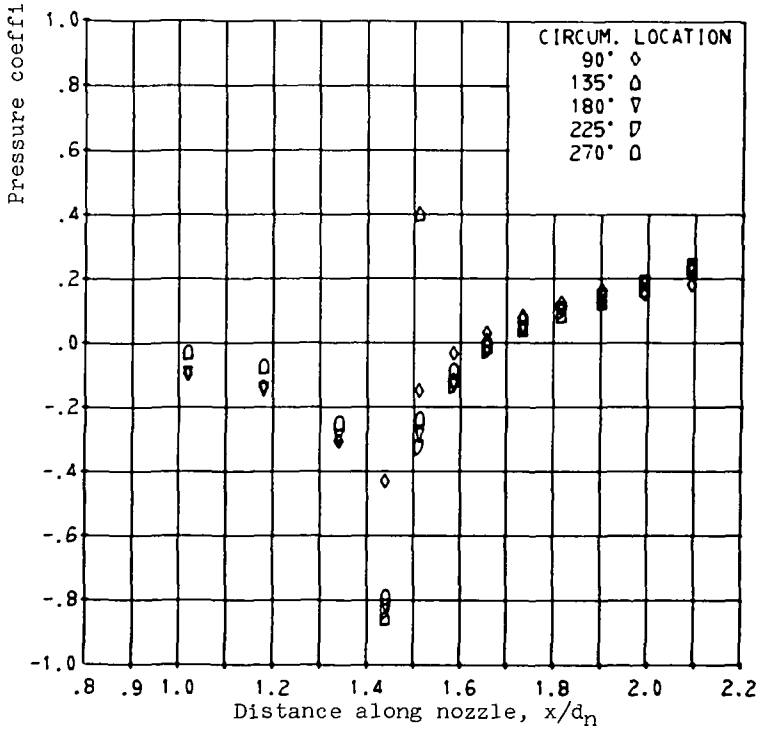

(c-2) Lower half.

(c) $M_0 = 0.890$; $d_9/d_8 = 1.18$; $\omega\sqrt{\tau} = 0.0434$.

Figure 20. - Continued.

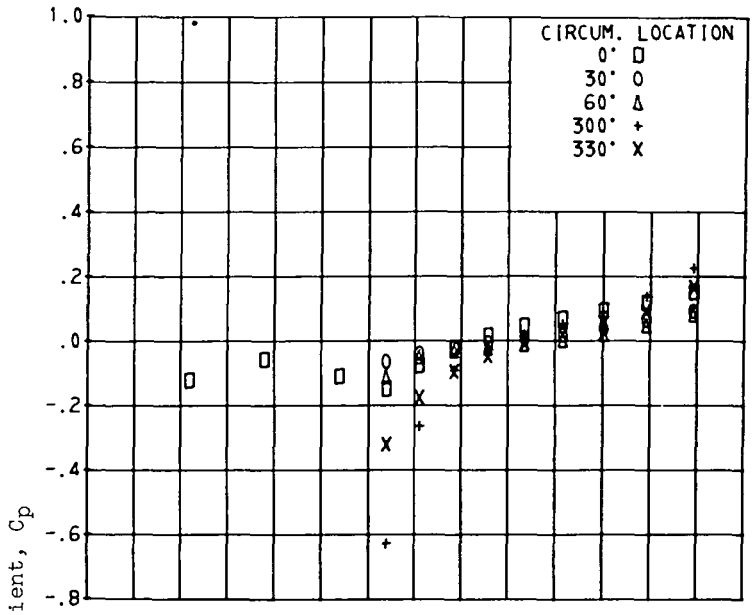

(d-1) Upper half.

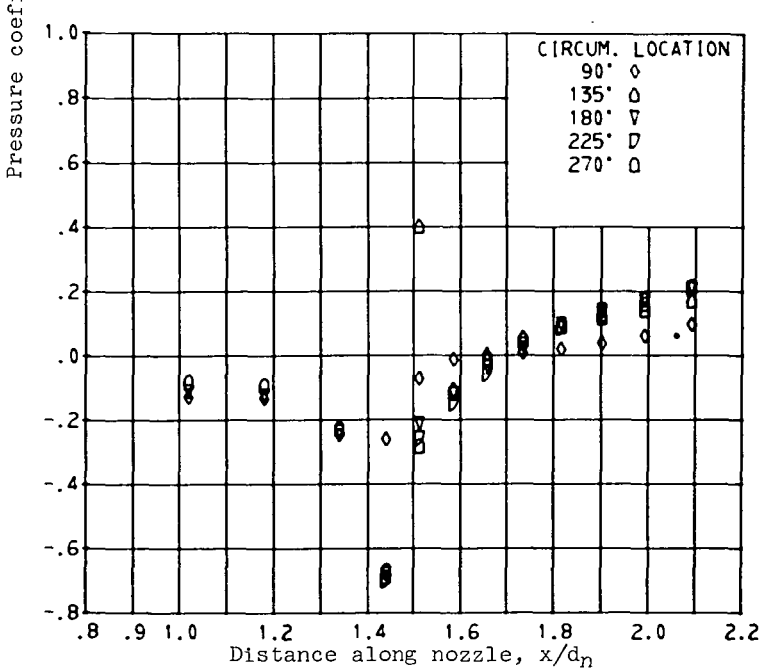

(d-2) Lower half.

(d) $M_0 = 0.958$; $d_9/d_8 = 1.18$; $\omega\sqrt{\tau} = 0.0422$.

Figure 20. - Continued.

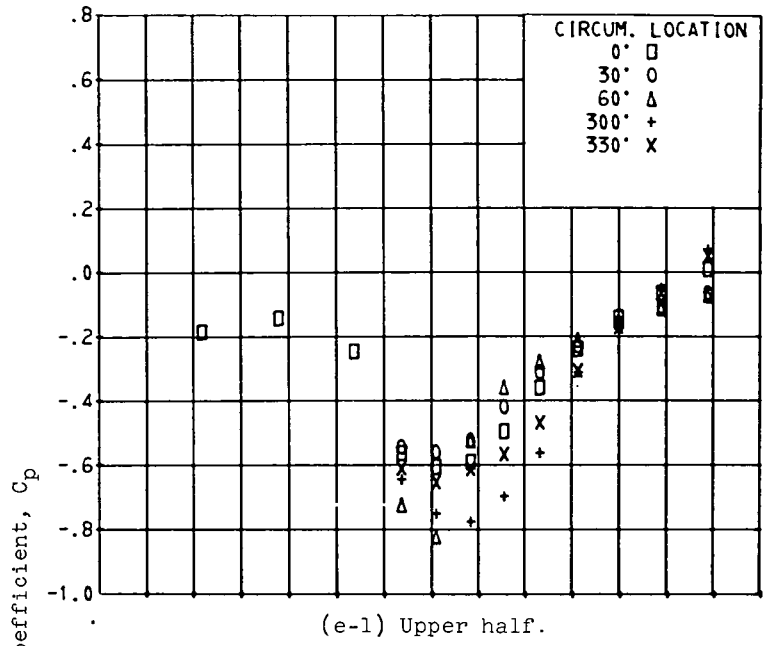

(e-1) Upper half.

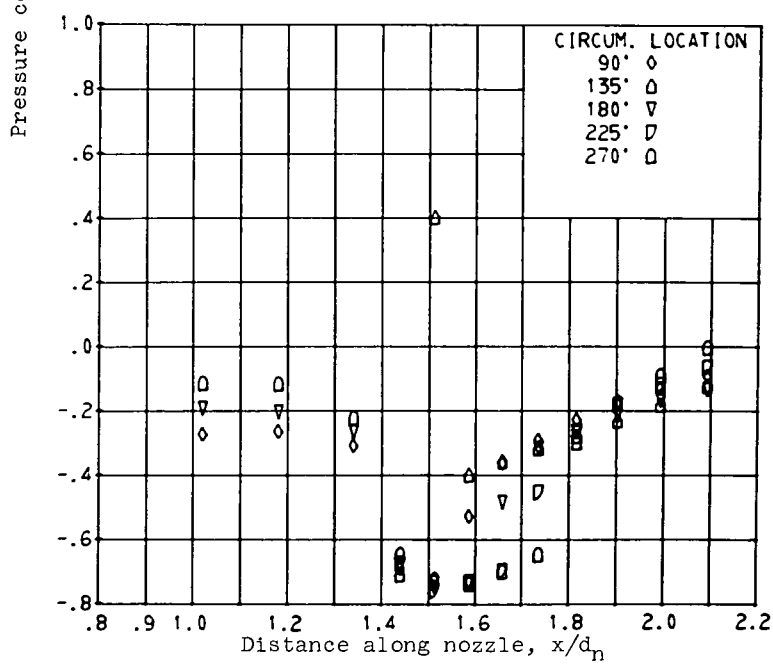

(e-2) Lower half.

(e) $M_0 = 1.011$; $d_9/d_8 = 1.19$; $\omega\sqrt{\tau} = 0.0632$.

Figure 20. - Continued.

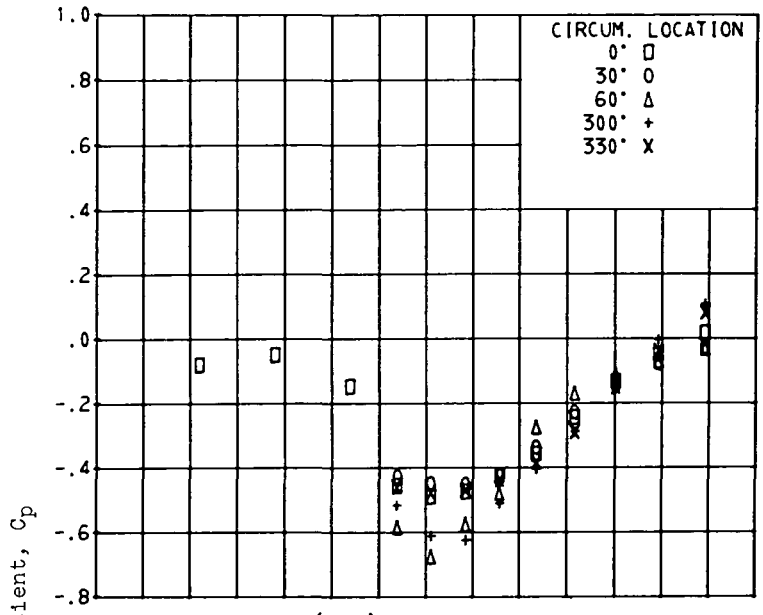

(f-1) Upper half.

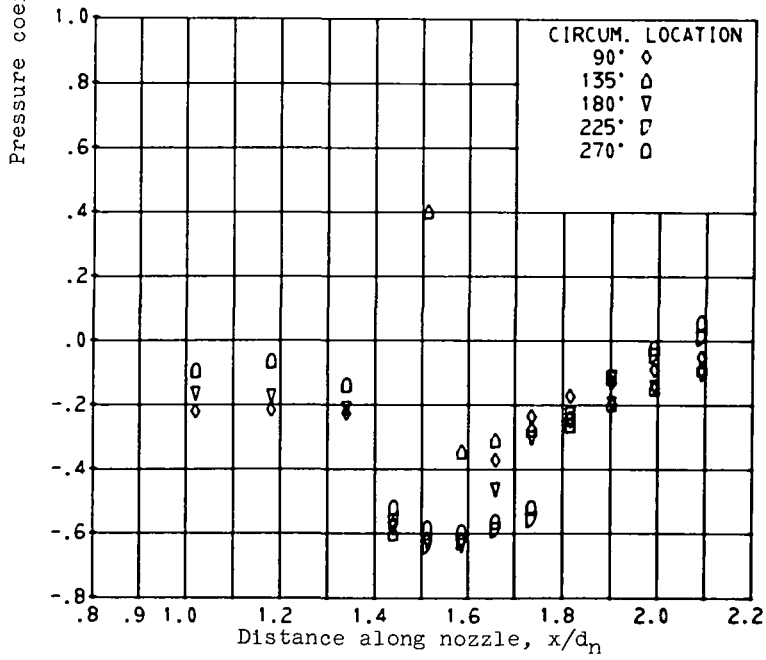

(f-2) Lower half.

(f) $M_0 = 1.085$; $d_9/d_8 = 1.17$; $\omega\sqrt{\tau} = 0.0435$.

Figure 20. - Concluded.

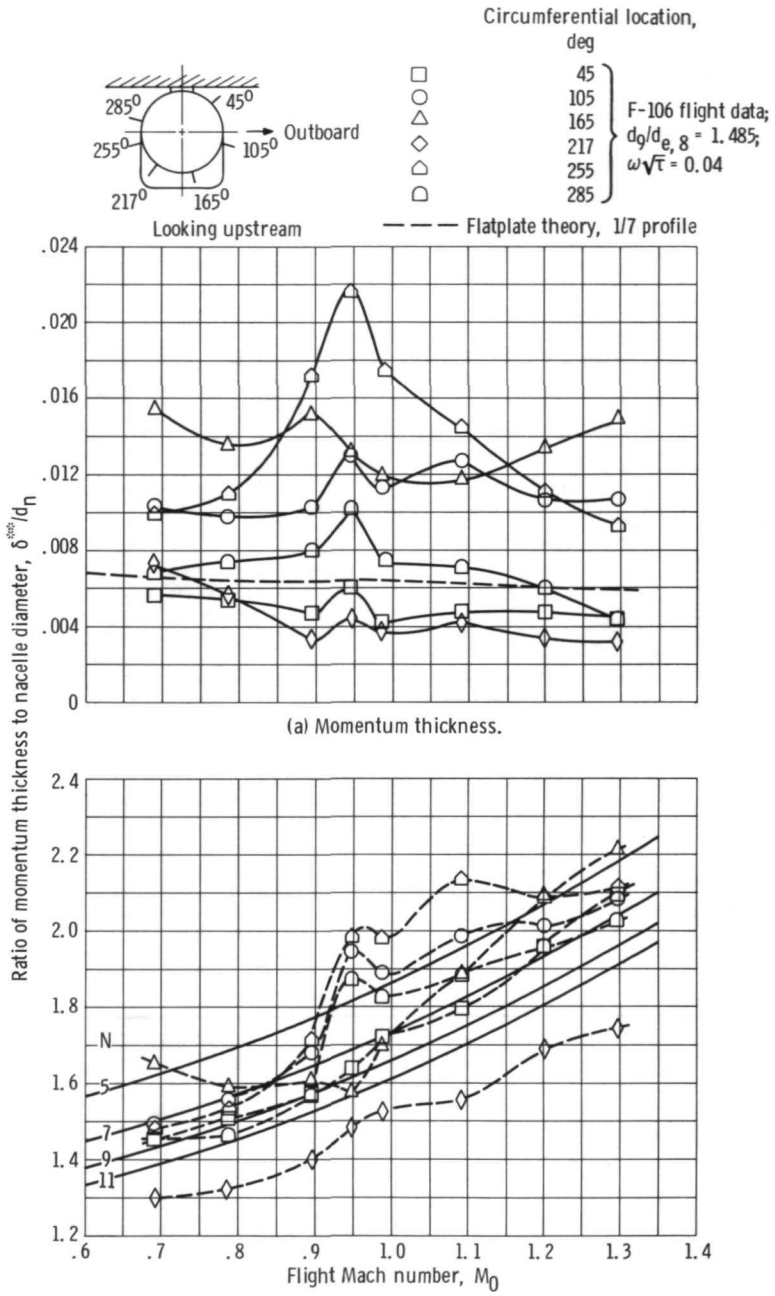

(a) Momentum thickness.

(b) Ratio of displacement to momentum thickness, showing exponent in boundary-layer velocity equation $V/V_{bl} = (z/\delta)^{1/N}$.

Figure 21. - Nacelle boundary-layer characteristics, nonreheat (military) power setting.

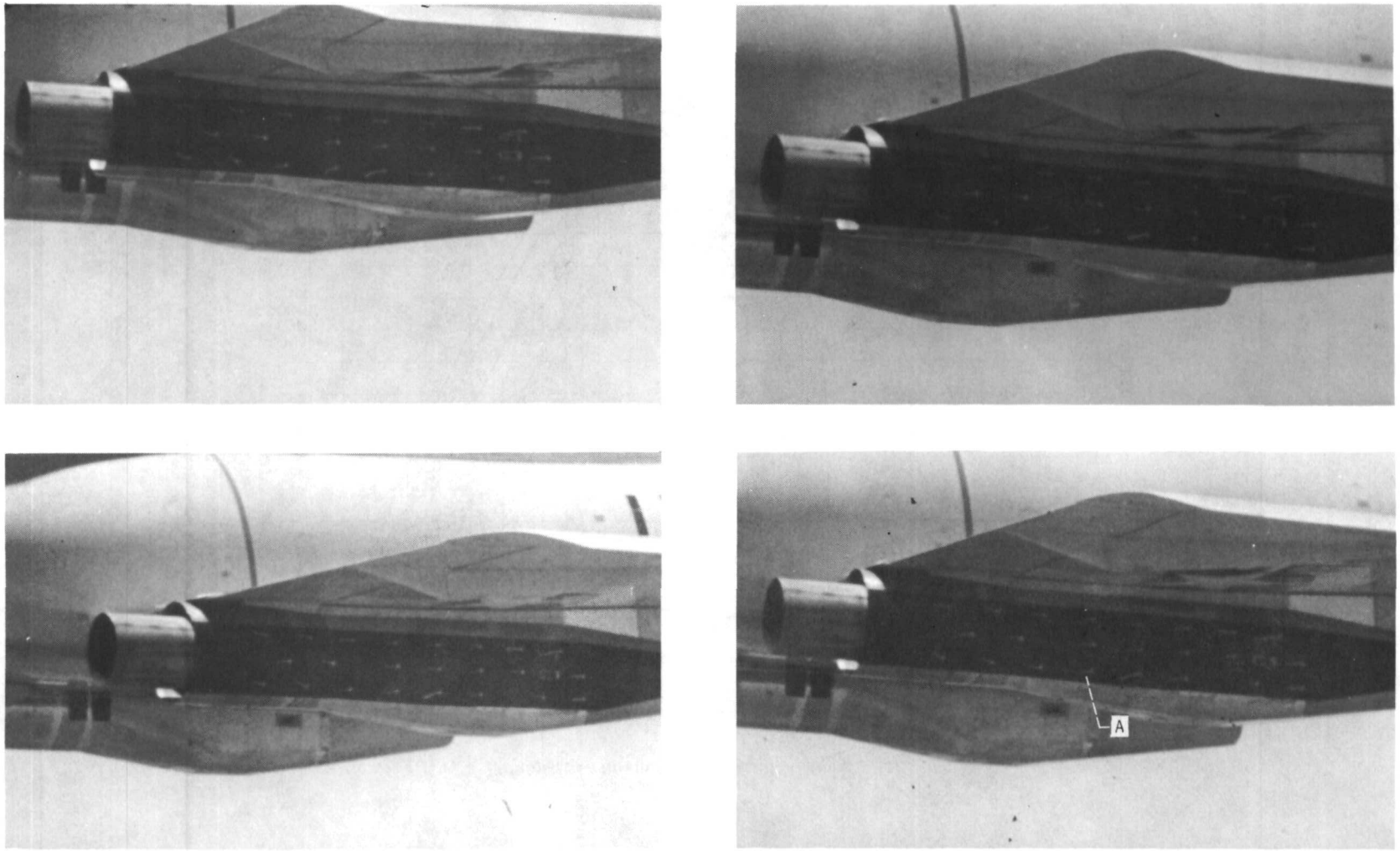

Figure 22. - Tufts showing flow direction and unsteady flow over underwing nacelles with a reference nozzle. Flight Mach number, 0.9.

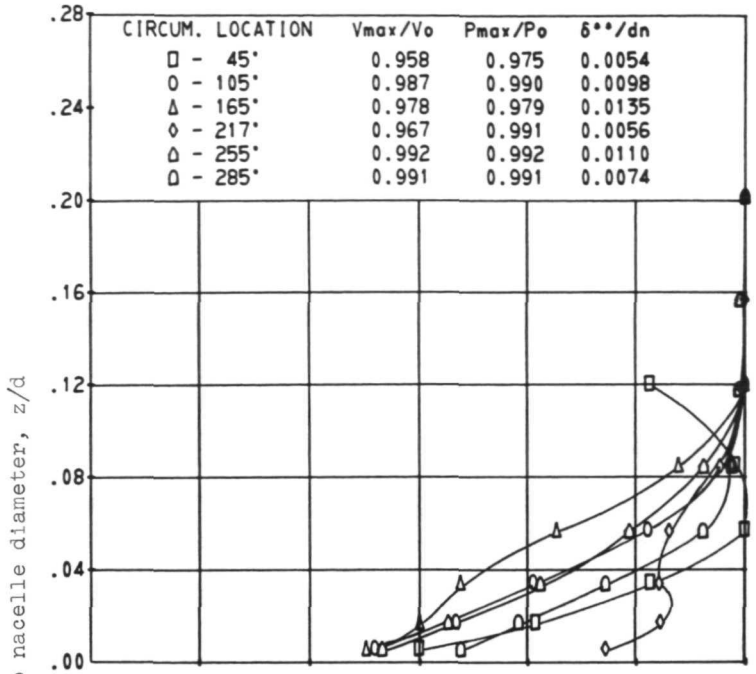

(a) $M_0 = 0.786$; $m_1/m_0 = 0.838$.

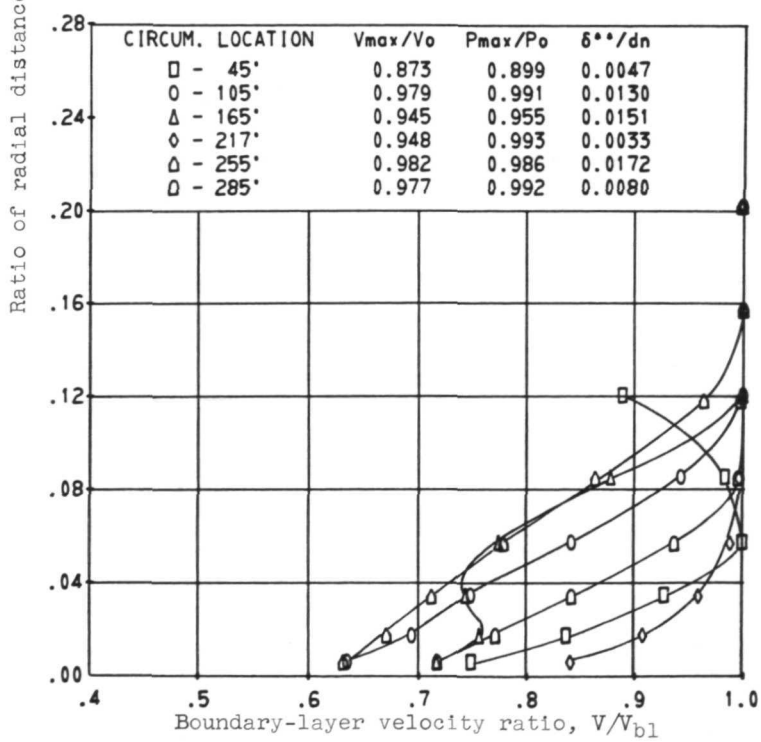

(b) $M_0 = 0.894$; $m_1/m_0 = 0.812$.

Figure 23. - Nacelle boundary-layer velocity profiles, for several values of flight Mach number M_0 and mass flow ratio m_1/m_0. Nonreheat (military) power setting; corrected secondary-weight-flow ratio, $\omega\sqrt{\tau} = 0.039$.

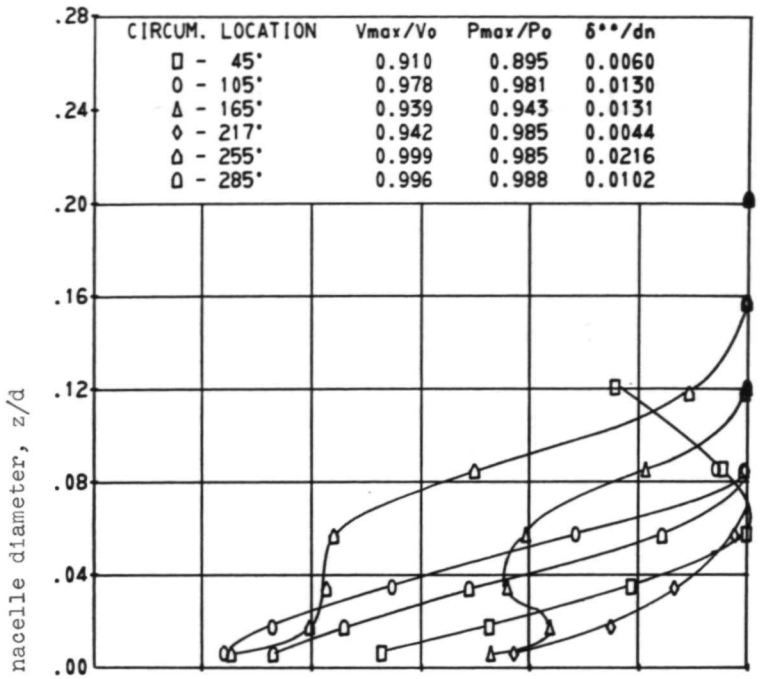

(c) $M_O = 0.946$; $m_1/m_O = 0.802$.

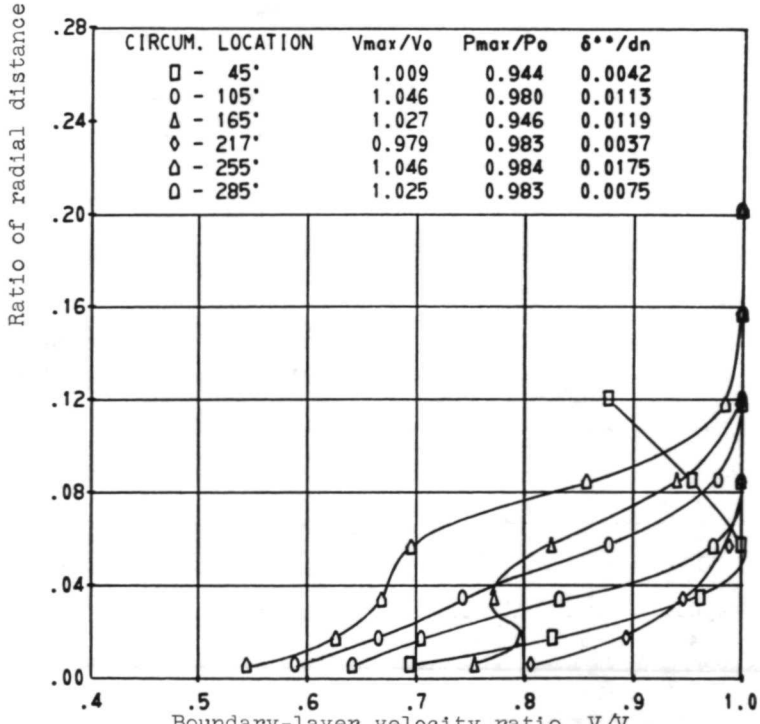

(d) $M_O = 0.986$; $m_1/m_O = 0.799$.

Figure 23. - Continued.

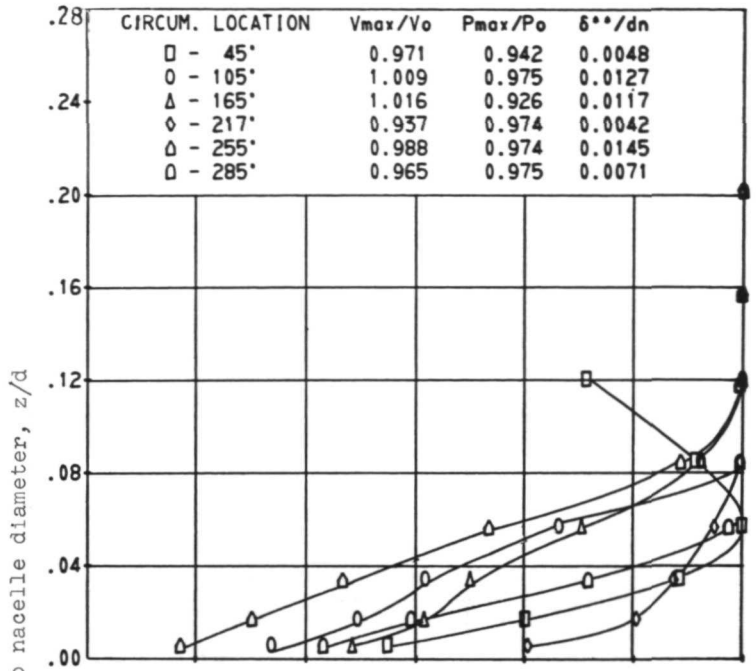

(e) $M_O = 1.090$; $m_1/m_O = 0.799$.

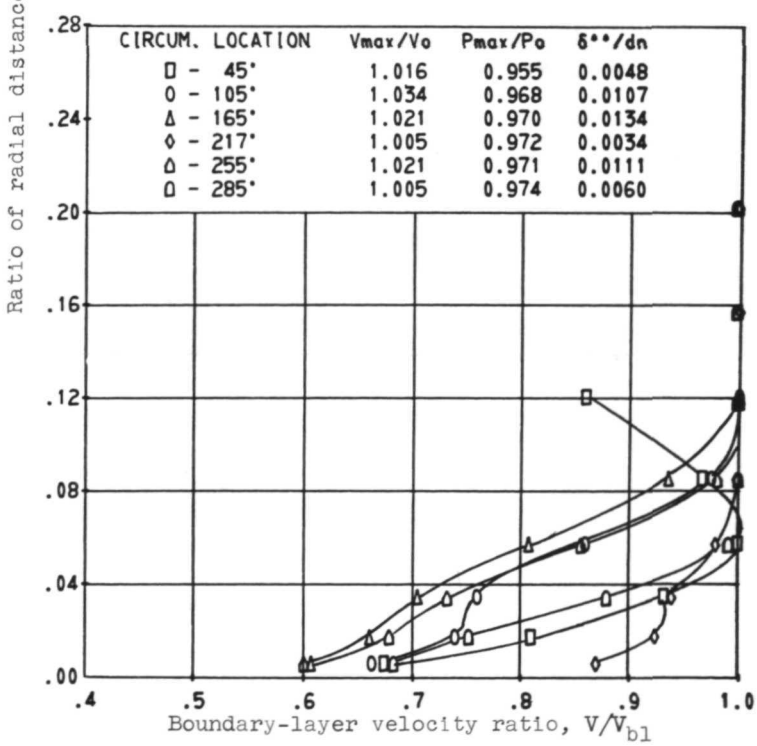

(f) $M_O = 1.199$; $m_1/m_O = 0.803$.

Figure 23. - Continued.

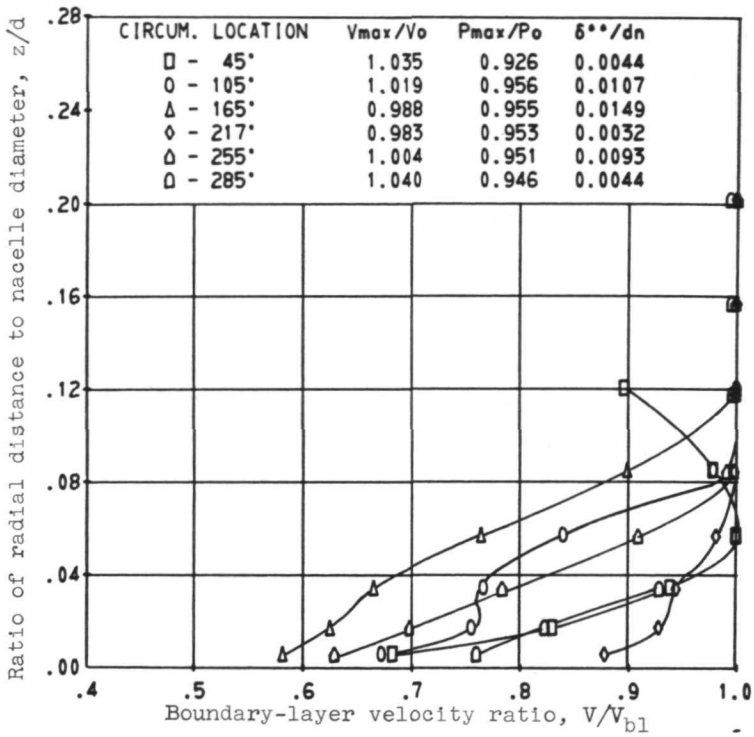

(g) $M_0 = 1.295$; $m_1/m_0 = 0.811$.

Figure 23. - Concluded.

NASA-Langley, 1972 —— 28 E-6564

NATIONAL AERONAUTICS AND SPACE ADMISTRATION
WASHINGTON, D.C. 20546

OFFICIAL BUSINESS
PENALTY FOR PRIVATE USE $300

FIRST CLASS MAIL

POSTAGE AND FEES PAID
NATIONAL AERONAUTICS AND
SPACE ADMINISTRATION

U.S.MAIL

POSTMASTER: If Undeliverable (Section 158 Postal Manual) Do Not Return

---

"The aeronautical and space activities of the United States shall be conducted so as to contribute . . . to the expansion of human knowledge of phenomena in the atmosphere and space. The Administration shall provide for the widest practicable and appropriate dissemination of information concerning its activities and the results thereof."

—NATIONAL AERONAUTICS AND SPACE ACT OF 1958

NASA SCIENTIFIC AND TECHNICAL PUBLICATIONS

TECHNICAL REPORTS: Scientific and technical information considered important, complete, and a lasting contribution to existing knowledge.

TECHNICAL NOTES: Information less broad in scope but nevertheless of importance as a contribution to existing knowledge.

TECHNICAL MEMORANDUMS: Information receiving limited distribution because of preliminary data, security classification, or other reasons.

CONTRACTOR REPORTS: Scientific and technical information generated under a NASA contract or grant and considered an important contribution to existing knowledge.

TECHNICAL TRANSLATIONS: Information published in a foreign language considered to merit NASA distribution in English.

SPECIAL PUBLICATIONS: Information derived from or of value to NASA activities. Publications include conference proceedings, monographs, data compilations, handbooks, sourcebooks, and special bibliographies.

TECHNOLOGY UTILIZATION PUBLICATIONS: Information on technology used by NASA that may be of particular interest in commercial and other non-aerospace applications. Publications include Tech Briefs, Technology Utilization Reports and Technology Surveys.

Details on the availability of these publications may be obtained from:

SCIENTIFIC AND TECHNICAL INFORMATION OFFICE

NATIONAL AERONAUTICS AND SPACE ADMINISTRATION

Washington, D.C. 20546